2021年11月11日(木)

A会場

インターナショナル sess.

[1A09-10] インターナショナル sess.(1)
座長:村山 徹(東京都立大学)
13:00 ～ 14:00 A会場 (函館アリーナ 会議室A)

[1A09] 【招待】脱水素的な分子転換プロセスの開発 –アルコール電解からメタン多量化まで–
○荻原 仁志[1]（1. 埼玉大学）
13:00 ～ 13:30

[1A10] [Invited] Precise synthesis, characterization, and reactivity of multi-functional catalysts
○Ro Insoo[1]（1. Seoul National University of Science and Technology）
13:30 ～ 14:00

インターナショナル sess.

[1A11-13] インターナショナル sess.(2)
座長:比護 拓馬(早稲田大学)
14:15 ～ 15:00 A会場 (函館アリーナ 会議室A)

[1A11] ゼオライト内インジウムヒドリド種の局所構造とエタン脱水素化能
○安村 駿作[1]、鳥屋尾 隆[1,2]、前野 禅[1]、清水 研一[1,2]（1. 北海道大学触媒科学研究所、2. 京都大学触媒電池）
14:15 ～ 14:30

[1A12] Au-Pt/ゼオライトを用いた0℃における高効率エチレン除去
○Lin Mingyue[1]、Wang Haifeng[1]、宍戸 哲也[1]、三浦 大樹[1]、春田 正毅[1]、村山 徹[1,2]（1. 東京都立大学、2. 煙台大学）
14:30 ～ 14:45

[1A13] Catalytic reduction of NO to ammonia by CO-H_2O over metal oxide supported catalysts
○Chaudhari Chaudhari Chandan[1], Keisuke Kobayashi[1], Yuichi Manaka[1,2], Tetsuya Nanba[1]（1. Fukushima Renewable Energy Inst., AIST , 2. Tokyo Inst. Tech. ）
14:45 ～ 15:00

インターナショナル sess.

[1A14-16] インターナショナル sess.(3)
座長:桑原 泰隆(大阪大学)
15:15 ～ 16:00 A会場 (函館アリーナ 会議室A)

[1A14] Low-temperature conversion of methane to methanol using carbon nanotubes supported catalyst
○Yingluo He[1], Guohui Yang[1], Noritatsu Tsubaki[1]（1. University of Toyama）
15:15 ～ 15:30

[1A15] CO_2吸着用 HKUST-1モノリスのワンポット合成
○酒井 求[1]、堀 隼太[2]、伊藤 綾香[3]、松本 隆也[4]、朝野 剛[4]、松方 正彦[1,2,3,5]（1. 早稲田大学ナノ・ライフ創新研究機構、2. 早稲田大学大学院先進理工学研究科応用化学専攻、3. 早稲田大学先進理工学部応用化学科、4. ENEOS株式会社、5. 早稲田大学理工学術院総合研究所）
15:30 ～ 15:45

[1A16] 火炎噴霧熱分解法により調製した Zr添加 Ni/CeO_2のCO_2メタン化反応活性
○藤原 翔[1]、榧野 宗悟[1]、吉岡 大[2]（1. 山形大学大学院 理工学研究科、2. 山形大学 工学部）
15:45 ～ 16:00

2021年11月12日(金)

A会場

インターナショナル sess.

[2A01-02] インターナショナル sess.(4)
座長:霜田 直宏(徳島大学)
09:00 ～ 10:00 A会場 (函館アリーナ 会議室A)

[2A01] [Invited] Heterogeneous catalytic conversion of C1 gas to value-added chemicals
○Baek Jayeon[1]（1. Korea Institute of Industrial Technology (KITECH)）
09:00 ～ 09:30

[2A02] 【招待】フェノールの酸化のためのマイクロポーラスチタノシリケート触媒の創製
○稲垣 怜史[1]（1. 横浜国立大学）
09:30 ～ 10:00

インターナショナル sess.

[2A03-05] インターナショナル sess.(5)
座長:田村 正純(大阪市立大学)
10:15 ～ 11:00 A会場 (函館アリーナ 会議室A)

[2A03] オレフィンメタセシス重合のためのイミド配位ニオブ錯体の合成と触媒活性への配位子効果
○Chatchaipaiboon Kanchana[1]、野村 琴広[1]（1. 東京都立大学）
10:15 ～ 10:30

[2A04] Depolymerization of Lignin by Using Ionic Liquid and Ethylene Glycol
○Peng Mingming[1]、Nakabayashi Manaka[1]、Qian Eika [1]（1. Tokyo University of Agriculture and Technology）
10:30 ～ 10:45

[2A05] Aerobic oxidation of concentrated acetal-

protected 5-HMF solutions to FDCA using nitrogen-doped carbon-supported cobalt as a non-noble metal catalyst

○Jan Wiesfeld[1], Atsushi Fukuoka[1], Kiyotaka Nakajima[1]
（1. iCAT, Hokkaido University）

10:45 ～ 11:00

インターナショナル sess.

[2A06-08] インターナショナル sess.(6)

座長:吉田 暁弘(弘前大学)
11:15 ～ 12:00 A会場 (函館アリーナ 会議室A)

[2A06] Sugars dehydration with Nb-based mixed metal oxide catalysts

○Daniele Padovan[1], Hideki Kato[2], Atsushi Fukuoka[1], Kiyotaka Nakajima[1] （1. Institute for Catalysis, Hokkaido University, 2. Institute of Multidisciplinary Research for Advanced Materials, Tohoku University）

11:15 ～ 11:30

[2A07] イオン性液体溶媒中での非環式ジエンメタセシス重合によるバイオベースポリエステルの合成

○王 秀々[1]、Zhao Weizhen[2]、野村 琴広[1] （1. 東京都立大学、2. 中国科学院　過程工程研究所）

11:30 ～ 11:45

[2A08] Reductive amination of 5-formyl-2-furancarboxylic acid to 5-(aminomethyl)furan-2-carboxylic acid

○Tat Boonyakarn[1], Jan J Wiesfeld[1], Atsushi Fukuoka[1], Takato Mitsudome[2], Kiyotaka Nakajima[1,3] （1. Institute for Catalysis, Hokkaido University, 2. Department of Materials Engineering Science, Graduate School of Engineering Science, Osaka University, 3. JST-MIRAI）

11:45 ～ 12:00

インターナショナル sess.

[2A09-10] インターナショナル sess.(7)

座長:大山 順也(熊本大学)
13:30 ～ 14:30 A会場 (函館アリーナ 会議室A)

[2A09] [Invited] Computational studies on atomic layer deposition mechanisms of Al_2O_3

○Kim Ki-Chul[1] （1. Konkuk University）

13:30 ～ 14:00

[2A10] 【招待】ハイスループット実験を基盤としたデータ駆動型触媒探索

○谷池 俊明[1] （1. 北陸先端科学技術大学院大学 先端科学技術研究科）

14:00 ～ 14:30

インターナショナル sess.

[1A09-10] インターナショナル sess.(1)

座長:村山 徹(東京都立大学)

2021年11月11日(木) 13:00 〜 14:00 A会場 (函館アリーナ 会議室A)

[1A09] 【招待】脱水素的な分子転換プロセスの開発　–アルコール電解からメタン多量化まで–

○荻原 仁志[1]（1. 埼玉大学）

13:00 〜 13:30

[1A10] [Invited] Precise synthesis, characterization, and reactivity of multi-functional catalysts

○Ro Insoo[1]（1. Seoul National University of Science and Technology）

13:30 〜 14:00

Dehydrogenative conversion of small molecules – from alcohol electrolysis to methane polymerization

(Saitama Univ.) ○ Hitoshi Ogihara

1. Introduction

The conversions of small molecules to value-added chemicals are important processes in the chemical industry. This presentation will show several dehydrogenative conversions processes. One is the electrolysis of lower alcohols. We have developed electrolysis systems for the conversion of lower alcohols into esters, aldehydes, and acetals.[1,2] The feature of the system is to use membrane electrode assembly (MEA) as an electrolysis unit. As shown in Fig. 1, alcohols converted into esters, aldehydes, and acetals on the anode. Then, proton and electron transfer through a proton-exchange membrane (PEM) and an external circuit, respectively. Finally, the proton and electron are recombined on the cathode to generate hydrogen. The electrolysis using MEA can be a sustainable process for upgrading alcohols to chemicals because it can use renewable electricity and does not require chemical reagents (e. g., oxidants and electrolytes).

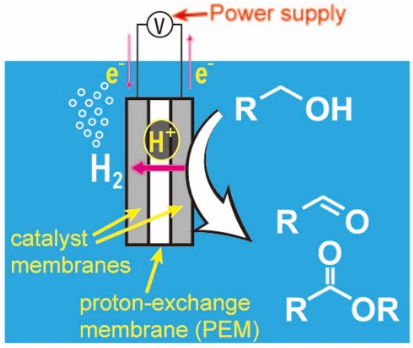

Fig. 1 Schematic diagram of electrolysis of alcohols using an MEA unit

Furthermore, we also studied the direct conversion of methane (CH_4) to C2 hydrocarbons and aromatics. CH_4 is expected to be used to produce essential chemicals, and recent developments in shale gas extraction technology are also supporting the use of natural gas in the chemical industry. However, CH_4, which is the main component of natural gas, is highly stable due to its strong C–H bond and symmetric molecular structure, making it difficult to convert it into useful chemicals. In this presentation, some approaches to activate CH_4 molecules are reported.

2. Results and Discussion

2.1 Electrolysis of alcohols using an MEA unit

We have proposed processes to convert alcohols into chemicals via the dehydrogenative electrolysis using an MEA device. One example is the electrolysis of methanol (CH_3OH). We found that the electrolysis of pure CH_3OH using the MEA device selectively produced methyl formate,[1] which is an important intermediate in the production of essential chemicals. The methyl formate and hydrogen are directly formed from CH_3OH according to Eqs 1 and 2. The average formation rate of methyl formate was 930 mmol h^{-1} g_{cat}^{-1} and a turnover frequency was 468 h^{-1}. The productivity of methyl formate via pure CH_3OH electrolysis was comparable to previously reported systems such as heterogeneous catalysts and photocatalysts.

$$\text{Anode:}\quad 2CH_3OH \rightarrow HCOOCH_3 + 4H^+ + 4e^- \qquad (1)$$
$$\text{Cathode:}\quad 2H^+ + 2e^- \rightarrow H_2 \qquad (2)$$

Next, we focused on ethanol (C_2H_5OH). The electrolysis of ethanol showed different behavior from CH_3OH electrolysis. In the electrolysis of pure C_2H_5OH, the main product was 1,1-diethoxyethane (DEE).[2] The formation scheme is shown in Fig. 2. Unlike CH_3OH, the electrochemical reaction of C_2H_5OH is mainly produced acetaldehyde as follows:

$$C_2H_5OH \rightarrow CH_3CHO + 2H^+ + 2e^- \qquad (3)$$

where a Pt/C acted as an electrocatalyst, then, acetaldehyde is converted into DEE with the aid of PEM (Nafion, in this study). Nafion is known as a strong acid catalyst so that the Nafion promotes the following acetalization reaction.

$$CH_3CHO + 2C_2H_5OH \rightarrow CH_3CH(OC_2H_5)_2 + H_2O \qquad (4)$$

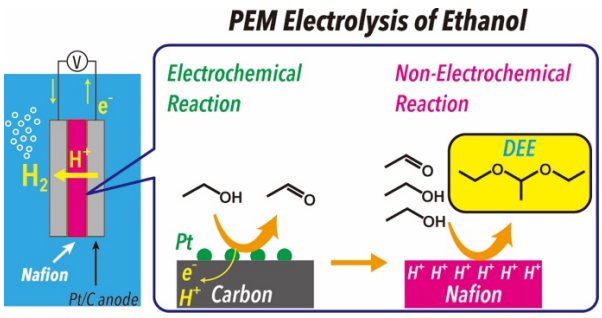

Fig. 2 Electrolysis of ethanol to form DEE.

DEE was produced at high faradaic efficiency (78 %) via the sequential electrochemical and nonelectrochemical reactions. The DEE formation rate was higher than that of previous reported systems.

So far, MEA has been widely used in the field of fuel cells and water electrolysis. Our work proposed that the MEA can be used as the electrolysis unit for upgrading alcohols into value-added chemicals (e.g., esters, aldehydes, and acetals).

2.2 Dehydrogenative polymerization of CH_4

Catalytic decomposition of CH_4 is a reaction that produces COx-free hydrogen.

$$CH_4 \rightarrow 2H_2 + C \quad (5)$$

We investigated the catalytic activity Pd-M alloy on the decomposition of CH_4 and found that Pd-Au and Pd-Si alloys promoted not only the decomposition of CH_4 but also coupling of CH_4 to produce C2 hydrocarbons.[3,4)]

$$2CH_4 \rightarrow C_2H_6 + H_2 \quad (6)$$

$$2CH_4 \rightarrow C_2H_4 + 2H_2 \quad (7)$$

Although the selectivity for C2 hydrocarbons was not so high (~2%), this is the first report that valuable C2 hydrocarbons can be co-produced during the decomposition of CH_4 to produce COx-free hydrogen.

In addition to the catalytic process, we proposed a new radical route to activate CH_4.[5)] CH_4 is so stable molecule that it cannot be activated without catalysts even at high temperatures. As shown in Table 1, CH_4 was not converted at 800 °C in the absence of catalysts. In contrast, ethane (C_2H_6) is more reactive than CH_4; therefore, C_2H_6 was dehydrogenated into C_2H_4 and C_6H_6 etc. In such a case, CH_4 is expected to be an inert gas; however, mixtures of CH_4/C_2H_6 and of Ar/C_2H_6 showed different pyrolysis behaviors; the addition of CH_4 increased the formation of propylene, propane and toluene. To reveal the activation process of CH_4, we used ^{13}C-labeled CH_4. Mass spectrometry analysis showed that carbon contained in CH_4 was incorporated into the pyrolysis products. We assumed that CH_4 was attacked by radical species generated from pyrolysis of C_2H_6 and was converted into methyl radicals (Fig. 3). The CH_4-derived methyl radicals were incorporated into pyrolysis products via radical reactions.

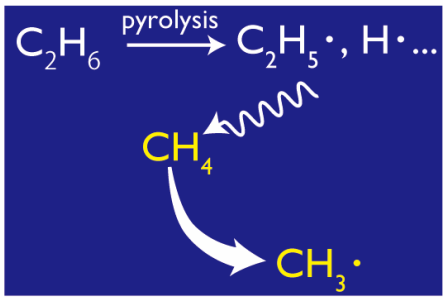

Fig. 3 Schematic diagram of CH_4 activation by radicals generated from the pyrolysis of C_2H_6.

3. Acknowledgement

This work was supported by JSPS KAKENHI (Grant Number 16K18287, 18K04832, and 21H01710), JST CREST (Grant Number JPMJCR15P4), the technology development project carried out in Japan Petroleum Energy Center (JPEC) under the commission of the Ministry of Economy, Trade and Industry (METI), and Tonen General Sekiyu Research/Development Encouragement & Scholarship Foundation.

References:

1) R. Kishi, H. Ogihara, M. Yoshida-Hirahara, K. Shibanuma, I. Yamanaka, H. Kurokawa, *ACS Sustain. Chem. Eng.*, **2020,** 8, 11532–11540.

2) D. Kawaguchi, H. Ogihara, H. Kurokawa, *ChenSusChem*, in press.

3) H. Ogihara, N. Imai, M. Yoshida-Hirahara, H. Kurokawa, *Chem. Lett.*, **2020**, 49, 236-239.

4) H. Ogihara, N. Imai, H. Kurokawa, *Int. J. Hydrog. Energy*, **2020**, 45, 33612-33622.

5) H. Ogihara, H. Tajima, H. Kurokawa, *React. Chem. Eng.*, **2020** ,48, 1145-1147.

Table 1 dehydrogenative conversion of CH_4, C_2H_6, and CH_4/C_2H_6. T = 1073 K, catalyst mass = 0 g.

reactant gas	yield / μmol h^{-1}								conv. / %	
	C_2H_4	C_2H_2	C_3H_8	C_3H_6	C_6H_6	C_7H_8	C_8H_8	$C_{10}H_8$	CH_4	C_2H_6
CH_4	1	n.d.	n.d.	n.d.	n.d.	n.d.	n.d.	n.d.	0.002	n/a
Ar/C_2H_6	13027	303	2	113	192	0.9	2	10	n/a	90.6
CH_4/C_2H_6	13611	266	24	595	125	3	2	4	-0.7	85.0

Precise Synthesis, Characterization, and Reactivity of Multi-functional Catalysts

Seoul National University of Science and Technology
Insoo Ro *

1. Introduction

Beyond the maximized atomic efficiencies and cost savings, atomically dispersed catalysts have attracted great attention in recent years due to the uniformity in active sites and careful regulation over local environments of active sites. Thus, it is interesting to investigate how the dispersed active site-support environment can be precisely engineered to control catalytic reactivity. In this work, we demonstrate control over the local coordination environment of atomically dispersed Rh on Al_2O_3 through a systematic tuning of interactions between Rh and ReO_x or WO_x species. Through this precise engineering of the local environment of atomically dispersed Rh species on an oxide support, it is shown that the local environment of the active site are significantly influenced, which in turn control ethylene hydroformylation reactivity. Whereas ReO_x were atomically dispersed on Al_2O_3 regardless of Re loading, the structure of WO_x on Al_2O_3 varied (atomically dispersed WO_x, polystungstate monolayer, to monoclinic WO_3 crystallites) by changing W loading, which influences the intrinsic reaction kinetics.

2. Experimental

Supported atomically dispersed Rh catalysts were prepared by a strong electrostatic adsorption method. Catalysts were characterized by a range of techniques, including UV-Vis and Raman spectroscopy, CO probe molecule infrared (IR), and transmission electron microscopy to understand the local structure and Rh charge state.

3. Results and Discussion

Figure 1 (a) and (b,c) show representative image of the Rh/ReO_x-Al_2O_3 and corresponding line scan intensity analysis of the two selected dimers, respectively. The difference in scattering intensity of Rh and Re species due to their different atomic mass (intensity α $Z^{1.5\text{-}2}$, where Z represents atomic number) evidences the formation of Rh-ReO_x atomically dispersed site pairs in Rh/ReO_x-Al_2O_3.

For ethylene hydroformylation, the propanal formation was greatly enhanced over Rh/ReO_x-Al_2O_3 and Rh/WO_x-Al_2O_3 relative to Rh/Al_2O_3, resulting in the higher selectivity toward propanal up to 63%. Interestingly, the selectivity toward propanal substantially changed depending on WO_x structure nearby dispersed Rh species. When Rh were localized with atomically dispersed WO_x (Rh/1WO_x-Al_2O_3), the selectivity toward propanal is the higher (63%) than Rh on bare Al_2O_3 (Rh/Al_2O_3, 22%), a polystungstate monolayer (Rh/2WO_x-Al_2O_3, 43%) and monoclinic WO_3 crystallites (Rh/8 and 25WO_x-Al_2O_3, 50%).

Kinetic experiments revealed that Rh/ReO_x-Al_2O_3 and Rh/WO_x-Al_2O_3 have higher CO reaction orders relative to Rh/Al_2O_3, indicating a decrease in the CO binding energy on Rh in Rh-ReO_x and Rh-WO_x co-localized structures, which was further evidence by CO temperature program desorption (TPD) characterization. This suggests that the promoted reactivity for Rh/ReO_x-Al_2O_3 and Rh/WO_x-Al_2O_3 was primarily due to an increase in the concentration of vacant sites under reaction conditions. As shown in Figure 2, the CO reaction orders increased and became positive over Rh/1 and 3WO_x-Al_2O_3, potentially suggesting that C_2H_4 adsorbed on atomically dispersed WO_x reacts with CO on nearby dispersed Rh. Two classes of active sites consisting of Rh and WO_x with an atomic intimacy allow a cooperative bifunctional mechanism when Rh is coordinated with atomically dispersed WO_x, consistent with previous report studies reporting atomically dispersed WO_x as active sites for olefin metathesis.

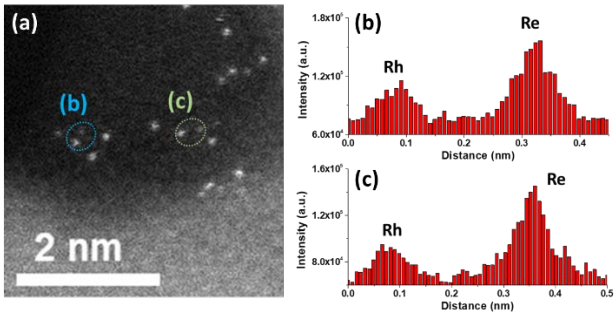

Figure 1. (a) HAADF STEM image of Rh/ReO_x-Al_2O_3. (b,c) Corresponding line scan intensity analysis of the two selected dimers shown in (a).

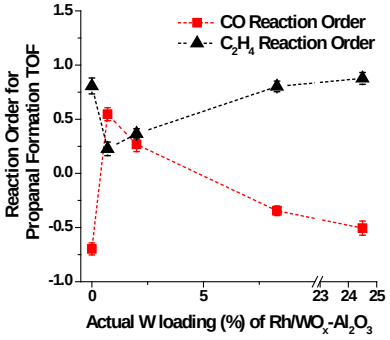

Figure 2. CO and C_2H_4 reaction orders for propanal formation TOF as a function of actual W loading of Rh/WO_x-Al_2O_3.

インターナショナル sess.

[1A11-13] インターナショナル sess.(2)

座長:比護 拓馬(早稲田大学)

2021年11月11日(木) 14:15 〜 15:00 A会場 (函館アリーナ 会議室A)

[1A11] ゼオライト内インジウムヒドリド種の局所構造とエタン脱水素化能

○安村 駿作[1]、鳥屋尾 隆[1,2]、前野 禅[1]、清水 研一[1,2] （1. 北海道大学触媒科学研究所、2. 京都大学触媒電池）

14:15 〜 14:30

[1A12] Au-Pt/ゼオライトを用いた0℃における高効率エチレン除去

○Lin Mingyue[1]、Wang Haifeng[1]、宍戸 哲也[1]、三浦 大樹[1]、春田 正毅[1]、村山 徹[1,2] （1. 東京都立大学、2. 煙台大学）

14:30 〜 14:45

[1A13] Catalytic reduction of NO to ammonia by CO-H_2O over metal oxide supported catalysts

○Chaudhari Chaudhari Chandan[1], Keisuke Kobayashi[1], Yuichi Manaka[1,2], Tetsuya Nanba[1] （1. Fukushima Renewable Energy Inst., AIST , 2. Tokyo Inst. Tech. ）

14:45 〜 15:00

Local structure of In-hydride species in zeolite and its reactivity for C_2H_6 dehydrogenation

(Institute for catalysis, Hokkaido University* · Elements Strategy Initiative for Catalysts & Batteries (ESICB), Kyoto University**)○Shunsaku Yasumura*, Takashi Toyao*,**, Zen Maeno*, Ken-ichi Shimizu*,**

1. Introduction

Hydrides in/on solid materials have attracted significant attention in many research fields, including energy engineering, electrochemistry, and catalysis. Research on the synthesis, characterization, and catalytic function of the isolated surface hydrides is an attractive but formidable task.[1] In this study, in-situ IR and DFT calculation were carried out to find the formation of isolated In-hydride species in indium-exchanged CHA zeolite (In-CHA).[2] The catalytic ability of In-CHA on C_2H_6 non-oxidative dehydrogenation was examined, resulting in superior selectively (96 %) and low coke formation during a long-term reaction (90h). By the combination of kinetic analysis and transition state (TS) calculation, it was elucidated that its catalytic performance was originated from the formation of not mono-hydride ($[InH]^{2+}$) but di-hydride species ($[InH_2]^{+}$) as active sites.

2. Experimental

In_2O_3 supported on the proton-type CHA (In_2O_3/CHA) was synthesized through impregnation of $In(NO_3)_3 \cdot nH_2O$ (Kanto Chemical Co., Inc.) in the NH_4^+-type CHA zeolite (Tosoh, SiO_2/Al_2O_3 = 22.3), followed by drying in an oven and calcination under air for 1 h at 773 K. Afterward, the reductive solid-state ion-exchange reaction of In_2O_3/CHA was conducted in the presence of H_2 at 773 K. For IR spectroscopic experiments, the In-CHA disk was prepared in-situ in a quartz reactor from a self-supported disk of In_2O_3/CHA. DFT calculations were performed using the Vienna ab initio simulation package (VASP) with a periodic boundary condition under the Kohn−Sham formulation.

3. Result and Discussion

The in-situ IR measurement of In-CHA treated with H_2 at 773 K (In-CHA(H_2)) was performed. The IR spectrum of In-CHA(H_2) exhibited a band with a maximum at 1720 cm^{-1} (Figure 1a) arising from In−H stretching vibrations (ν(In−H)). This band remained unchanged even at 473 K. After H−D exchange reaction with D_2 at 373 K, ν(In−H) decreased and disappeared at 473 K. ν(In−H) appeared again by the following exposure to H_2 at 473 K. The gas-phase products were also analyzed by mass spectrometry during the H−D exchange reaction with an increase in the temperature from 313 to 473 K. The reaction of In-CHA(H_2) with D_2 afforded a positive peak for m/z = 3 with a negative peak for m/z = 4 around 373−473 K (Figure 1b), while a peak for m/z = 2 was hardly observed. A control experiment using proton-type CHA (H-CHA) instead of In-CHA (H_2-treated H-CHA with D_2) was conducted where no peak was observed for all signals, supporting the occurrence of an H−D exchange reaction between In-hydrides and D_2.

In-CHA exhibited high selectivity (96 %) and durability for the nonoxidative ethane dehydrogenation without cofeeding of H_2. The activity and selectivity of In-CHA were maintained for at least 90 h, and the catalyst was reusable without loss of its efficiency. Based on the results of kinetic analysis and TS calculations, the formation of $[InH_2]^+$ as active sites is responsible for the durable reaction due to the less formation of Bronsted acid sites and carbenium cations. More detailed reaction mechanisms and the relationship with the local structure of In-hydride species will be discussed

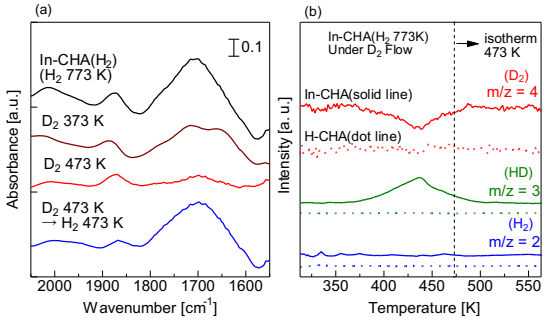

Figure 1 (a) FTIR spectra of In-CHA after H_2 treatment at 773 K (In-CHA(H_2)) and H−D exchange reactions. (b) Mass profiles for m/z = 2, 3, and 4 during H−D exchange reaction of In-CHA(H_2) (solid line) or H-CHA(H_2) (dot line) with D_2.

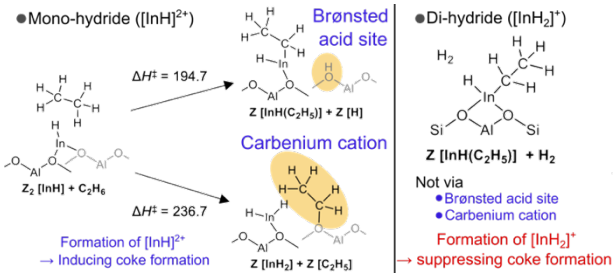

Figure 2 Reaction scheme of non-oxidative dehydrogenation of C_2H_6 on indium mono-hydride ($[InH]^{2+}$) and di-hydride ($[InH_2]^{+}$) species in zeolite.

References

1 C. Copéret, D. P. Estes, K. Larmier and K. Searles, *Chem. Rev.*, 2016, **116**, 8463.

2 Z. Maeno, S. Yasumura, X. Wu, M. Huang, C. Liu, T. Toyao and K. Shimizu, *J. Am. Chem. Soc.*, 2020, **142**, 4820.

Highly efficient removal of ethylene at 0 °C over Au-Pt/zeolite

([1]Tokyo Metropolitan University, [2]Yantai University)
○Mingyue Lin[*1], Haifeng Wang[*1], Tetsuya Shishido[*1], Hiroki Miura[*1], Masatake Haruta[*1], Toru Murayama[*1,2]

1. Introduction

Ethylene (C_2H_4) released from the plants could fasten the mature and deterioration of fresh fruits and vegetables even at low temperatures since it is a natural gaseous plant hormone. To prolong the storage time of the fresh plants during the transportation, removing trace amounts of C_2H_4 is important, and selective catalytic oxidation of C_2H_4 to CO_2 is an ideal method.[1] However, almost all of the reported catalysts would be deactivated due to the water adsorption, usually within 1 h. Therefore, it is necessary to develop a more effective material with a high C_2H_4 removal efficiency and long-term stability at low temperatures (0~5 °C).

Here, we report an Au-Pt/zeolite (ZHM20) with a highly active C_2H_4 removal efficiency (81%) and long-term stability (40 h) for C_2H_4 elimination at 0 °C.

2. Experimental

Mordenite 20 (ZHM20, SiO_2/Al_2O_3=18.3) provided by the Catalysis Society of Japan was used as the support. The loading amount of nanoparticles was prepared as 1wt%. Sol immobilization method[2] was applied to prepare ZHM20, Pt/ZHM20, Au/ZHM20, and Au_xPt_y/ZHM20 (x and y represent the molar ratio of Au and Pt, respectively) and they were calcined at 500 °C for 2 h before being used.

A fixed-bed flow reactor was used to conduct the C_2H_4 removal test. The sample (0.2 g) was firstly pretreated at 150 °C for 2 h under N_2 with a flow rate of 50 mL min^{-1} before being evaluated under the reactant gas that contained 50 ppm C_2H_4, 20% O_2, and N_2 balance with a total flow rate of 10 mL min^{-1}. The inlet and outlet concentrations of C_2H_4 and CO_2 were analyzed by an online 490 Micro GC system (Agilent) for calculating the removal efficiency of C_2H_4 and the yield of CO_2.

3. Results and Discussion

As shown in Figure 1, the initial C_2H_4 removal efficiency over ZHM20 was 100% at 0 °C and it reached the maximum adsorption capacity after flowing 11 h of 50 ppm C_2H_4. The removal efficiency curves of Pt/ZHM20 and Au/ZHM20 were U-shaped. Initially, the removal efficiency was 100% and it decreased to 19% and 15% after 10 h-on-stream over Pt/ZHM20 and Au/ZHM20, respectively, which was the same with that observed from ZHM20, suggesting that this step might be owing to the adsorption of C_2H_4 on ZHM20. Then, the C_2H_4 removal efficiency increased until reaching the steady-state of 56% on Pt/ZHM20 and 45% on Au/ZHM20. $Au_{54}Pt_{46}$/ZHM20 also showed a U-shape removal efficiency curve, but the turning point time of 3.5 h was much shorter than the other two. Moreover, the C_2H_4 removal efficiency of $Au_{54}Pt_{46}$/ZHM20 at the steady-state was 81% and it lasted for as long as 40 h. According to the electronic state analysis, $Au_{54}Pt_{46}$/ZHM20 possessed electron-deficient Pt species and electron-rich Au species, which might be helpful for the faster adsorption and transformation of C_2H_4 on $Au_{54}Pt_{46}$ NPs than that on Au NPs and Pt NPs.

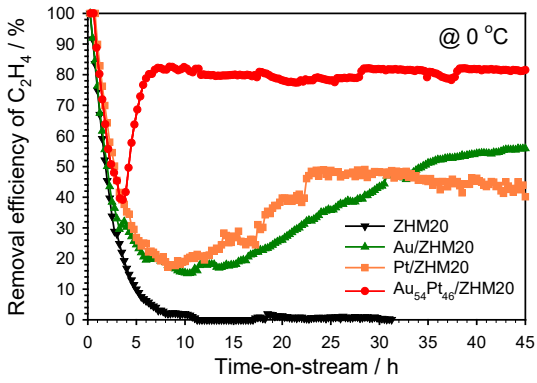

Figure 1. The removal efficiency of C_2H_4 with time-on-stream over ZHM20, Au/ZHM20, Pt/ZHM20, and $Au_{54}Pt_{46}$/ZHM20 at 0 °C.

1) C. Jiang, K. Hara, A. Fukuoka, Angew. Chem. Int. Ed., 52(24), 6265 (2013)
2) H. Miura, Y. Tanaka, K. Nakahara, Y. Hachiya, K. Endo, T. Shishido, *Angew. Chem. Int. Ed.*, 130(21), 6244 (2018)

Catalytic reduction of NO to ammonia by H_2 or CO-H_2O over metal oxide supported catalyst.

(FREA[1], TIT$_2$) ○C. Chaudhari,[1] K. Kobayashi,[1] Y. Manaka[1,2*] T. Nanba[1]

1.Introduction

Ammonia is an important *N*-containing chemical which is used as fertilizer, starting material for heterocycles sthe synthesis and carbon-free fuel. Ammonia is synthesized industrially by Haber-Bosch method with high energy consumption. Ammonia synthesis from air pollutant NO is an attractive alternative to reduce the concentration of NO. Several reductants such as hydrocarbon, H_2 or CO-H_2O have reported for the transformation of NO to NH_3. Recently, our group developed Pt/TiO_2 catalyst for ammonia synthesis on NO-CO-H_2O reaction.[1] However, the activity of Pt/TiO_2 was not studied for NO-H_2 reaction. In this study, we investigated and optimized the catalytic activity of Pt/TiO_2 for NH_3 synthesis. Furthermore, the activity of Cu/CeO_2 catalyst at lower temperature (>200 °C) investigated for NO-CO-H_2O reaction.

2. Experimental

Supported metal catalysts were prepared by an incipient wetness method with different Pt or Cu precursors. TiO_2 or CeO_2 support was prepared by sol-gel method using different conditions. All catalysts were characterized by BET and CO adsorption. The catalytic activity was measured by a fixed-bed flow reactor. For NO-H_2 reaction, the feed gas was composed of 0.1 % NO, 0.3% H_2 ppm with dilution by Ar. For NO-CO-H_2O reaction, the feed gas was composed of 0.1 % NO, 0.3% CO and 1% H_2O ppm with dilution by Ar. The total flow was set to 250 mL/min. The product gases were analyzed online Fourier transform infrared spectroscopy and gas chromatography.

3. Results and Discusion

Initially, we synthesized Pt/TiO_2 catalyst using different precursor such as $(NH_3)_4Pt(NO_3)_2$, $(NH_3)_4Pt(Cl)_2$, $(NH_3)_4Pt(OH)_2$ and H_2PtCl_6 and tested for NO-H_2 reaction. All precursors showed full conversion (100 %) of NO. The catalytic activity of all four precursors for ammonia selectivity was almost similar at lower temperature (100 °C-150 °C). When the temperature increased to 230 °C, H_2PtCl_4 showed superiority (99 %) for the synthesis of ammonia (Fig.1). Later, we investigated the effect of reduction temperature using different temperatures (400 °C, 500 °C and 600 °C). When Pt/TiO_2 catalyst prepared from H_2PtCl_4 precursor reduced at 400 °C, high yield of ammonia (98.9%) was obtained at 230 °C.

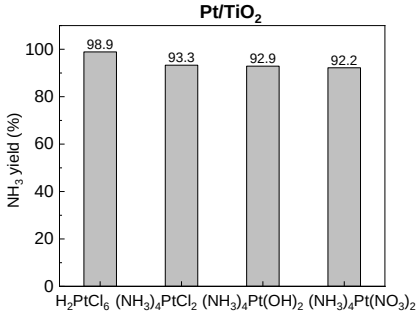

Fig. 1. The activity of Different Pt catalysts at 230 °C

For NO-CO-H_2O reaction, we examined Cu/CeO_2 catalysts prepared from different precursors at 150 °C. The catalyst prepared from $Cu(NO_3)_2$ precursor showed higher yield (72%) than other precursors.

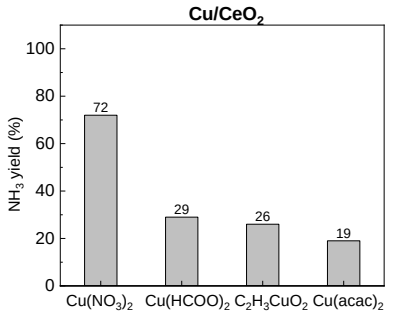

Fig. 2. The activity of Different Pt catalysts at 150 °C

In summary, Pt/TiO_2 prepared from H_2PtCl_6 found to be an active catalyst for ammonia synthesis over NO-H_2 reaction. In NO-CO-H_2O reaction, Cu/CeO_2 catalyst showed high activity for ammonia synthesis.

[1]K. Kobayashi, R. Atsumi, Y. Manaka, H. Matsumoto, T. Nanba, *Catal. Sci. Technol.,* **9**, 289 (2019).

インターナショナル sess.

[1A14-16] インターナショナル sess.(3)

座長:桑原 泰隆(大阪大学)

2021年11月11日(木) 15:15 〜 16:00 A会場 (函館アリーナ 会議室A)

[1A14] Low-temperature conversion of methane to methanol using carbon nanotubes supported catalyst

○Yingluo He[1], Guohui Yang[1], Noritatsu Tsubaki[1] （1. University of Toyama）

15:15 〜 15:30

[1A15] CO_2吸着用 HKUST-1モノリスのワンポット合成

○酒井 求[1]、堀 隼太[2]、伊藤 綾香[3]、松本 隆也[4]、朝野 剛[4]、松方 正彦[1,2,3,5] （1. 早稲田大学ナノ・ライフ創新研究機構、2. 早稲田大学大学院先進理工学研究科応用化学専攻、3. 早稲田大学先進理工学部応用化学科、4. ENEOS株式会社、5. 早稲田大学理工学術院総合研究所）

15:30 〜 15:45

[1A16] 火炎噴霧熱分解法により調製した Zr添加 Ni/CeO_2の CO_2メタン化反応活性

○藤原 翔[1]、樫野 宗悟[1]、吉岡 大[2] （1. 山形大学大学院　理工学研究科、2. 山形大学　工学部）

15:45 〜 16:00

Low-temperature conversion of methane to methanol using carbon nanotubes supported catalyst

(University of Toyama) ○Yingluo He, Guohui Yang, Noritatsu Tsubaki

1. Introduction

Conversion of methane to methanol is performed by a two-step process under harsh reaction conditions in industry. The direct synthesis process of methanol from partial oxidation of methane has been studied for a few decades. However, it remains one of the considerable challenges in the sector of methane utilization. [1] Herein, we report carbon nanotubes (CNTs) supported palladium-gold (Pd-Au) nanoparticles catalyst for this direct synthesis, which shows outstanding methanol selectivity and productivity at low temperature. [2), 3)]

2. Experimental

2.1 Catalyst preparation

Commercial CNTs were pretreated by various acids to modify its surface properties. The supported Pd-Au catalysts were prepared by an incipient wetness impregnation method. The Pd and Au amount were 2.5 % wt respectively without explain.

2.2 Catalyst characterization

XRD, XPS, H_2-TPR, CO-PULSE, FE-SEM, HR-TEM measurements were performed to analyze the physical and chemical properties of our catalysts.

2.3 Catalytic tests

Catalyst tests for direct synthesis of methanol from methane were accomplished in a stainless-steel autoclave. The motor was vigorously stirred at 1200 rpm, the temperature was raised to 50 °C to start the reaction at the same time. After the 30 min reaction, the vessel was cooled by ice (< 10 °C), to avoid volatilization of the products.

3. Results and Discussion

The carbon materials such as carbon nanotubes (CNTs), activated carbon (AC), and reduced graphene oxide (rGO) are employed as the catalyst support, and the palladium-gold (Pd-Au) nanoparticles are used as active center. By using oxygen/hydrogen mixture as oxidant in the direct synthesis, it is found that Pd-Au/CNTs catalyst shows outstanding methanol selectivity and productivity.

Table 1 Catalytic performance with different carbon supported Pd-Au nanoparticles catalyst

Catalyst	Total product ($mmol/kg_{cat.}$)	MeOH Selectivity (%)	TON of MeOH [b]
Pd-Au/rGO	33.2	54.2	76.5
Pd-Au/AC	156.0	65.6	435.1
Pd-Au/CNTs	190.1	73.2	591.7
Pd-Au/CNTs-a	149.5	71.2	452.6
Pd-Au/CNTs-n	98.0	90.0	375.0

a: Reaction conditions: Time 30 min; Temp. 50 °C; Solvent H_2O 10 mL; Catalyst weight 30 mg; Feed gas $CH_4/O_2/H_2/Ar$; Total pressure 3.3 MPa.
b: mmoles of MeOH formed by per mole Pd metal.

Compared with the Pd-Au/CNTs, the Pd-Au/CNTs-n catalyst with a treatment of nitric acid on the CNTs support enhances the methanol selectivity obviously (Table 1), due to the changed surface oxygen species on the supports. In addition, our characterization results reveal that a weak interaction between Pd-Au nanoparticles and CNTs support is in favor of methanol productivity and selectivity.

This work offers a simple and effective strategy to directly synthesize methanol from methane partial oxidation under the mild conditions.

1) Hammond C, Forde M. M, Ab Rahim M. H, et al.; *Angew. Chemie - Int. Ed.*, **51**, 5129 (2012).
2) He Y, Luan C, et al.; *Catalysis Today*, **339**, 48 (2020).
3) He Y, Liang J, et al.; *Catalysis Today*, **352**, 104 (2020).

One-pot synthesis of HKUST-1 monolith for CO_2 adsorption

CO_2吸着用 HKUST-1 モノリスのワンポット合成

(早大ナノ・ライフ*・早大先進理工**・ENEOS 株式会社***・早大理工総研****)
○酒井 求(さかいもとむ)*・堀隼太(ほりはやた)**・伊藤綾香(いとうあやか)**・松本隆也(まつもとたかや)***・朝野 剛(あさのつよし)***・松方正彦(まつかたまさひこ)*, **, ****

1. Introduction

Metal-organic-framework (MOF) is drawn attention as CO_2 adsorbent. Shape forming technology for powdery MOF is required in order to generate objects of millimetric dimensions with enough mechanical resistance for application in industry[1]. In this study, alumina tube and Cu cube were used as the metal source for MOF preparation and a part of them was directly converted into MOF monoliths. The preparation method of MOF monolith and its adsorption property were investigated.

2. Experimental

Two types of monoliths containing MOFs, HKUST-1 and MIL-96, were prepared. HNO_3, trimesic acid (TMA), and porous α-alumina tube were used as raw materials for MIL-96 preparation. Porous Cu cube was used for HKUST-1 preparation instead of α-alumina tube. Either alumina tube or Cu cube was placed into the aqueous solution of HNO_3 and TMA, and then hydrothermally treated by using glass-lined autoclave. The effect of these preparation conditions on the preparation of MOF monolith was studied.

MIL-96 powder was synthesized according to the literature[2] as reference material. HKUST-1 powder (Basolite C-300) was purchased from Sigma-aldrich.

CO_2 adsorption properties of prepared MOF powder and monoliths were measured by volumetric adsorption method (Belsorp-MAX, microtracBEL).

3. Results and discussion

The concentrations of HNO_3 and TMA and the conditions of hydrothermal treatment were widely changed. By the optimization of synthesis conditions, the contents of MIL-96 and HKUST-1 in monoliths increased up to 6.0 and 32 wt%, respectively.

Fig. 1 shows the morphological features of raw materials of metal sources and monoliths synthesized. The surface of alumina tube was fully covered with MIL-96 crystals and the color of alumina tube changed to yellow. The surface of Cu cube was converted to HKUST-1 as well.

Fig. 2 shows the isotherms of CO_2 on MIL-96 and HKUST-1 monoliths and powders at 298 K. The adsorbed amount of CO_2 at 100 kPa on MIL-96 monoliths and powder were 140 and 95 cm^3(STP) g^{-1}, respectively. HKUST-1 powder and monolith showed almost the same values of the CO_2 adsorbed amount, 99 cm^3(STP) g^{-1}.

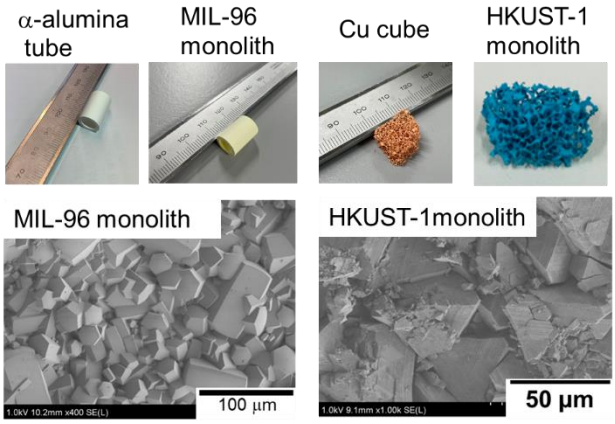

Fig. 1 Typical photo and FE-SEM images of α-alumina, MIL-96 monolith, Cu cube and HKUST-1 monolith.

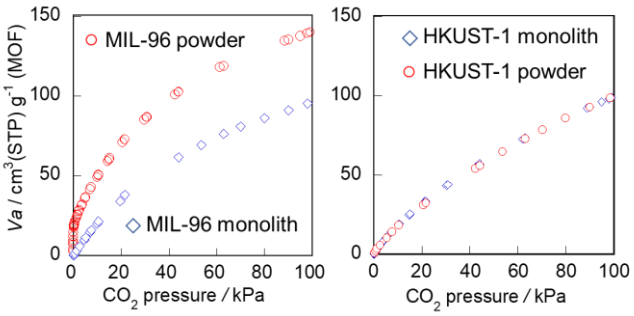

Fig. 2 CO_2 isotherms on MIL-96 and HKUST-1 at 298 K.

References

1) Bazer-Bachi, D., *et al., Powder Technol.*, **255** (2014) 52-29.
2) Benoit, V. *et al., J. Mater. Chem. A*, **6** (2018) 2081-2090.

Zr doped Ni/CeO_2 prepared by Flame spray pyrolysis for CO_2 methanation

(Yamagata University) Kakeru Fujiwara*, Syugo Kayano and Dai Yoshioka

1. Introduction

Utilization of CO_2 by converting it into CH_4 is sought because it reduces CO_2 emission to the environment and stores H_2 produced by renewable energies. So far, for this reaction, Ru supported on CeO_2 is one of the most active catalyst but its utilization is limited due to the cost of Ru. Alternatively, Ni has attracted the interest but it suffers from the low activity at low temperature (< 250 ºC) compared to Ru catalysts. To address the issue, high Ni loading with keeping the size small is promising approach for maximizing the Ni surface area. Here, we successfully prepared highly-loaded NiO (60 wt% as Ni) on CeO_2 nanoparticles by flame spray pyrolysis (FSP). Furthermore, the effect of Zr doping to the Ni/CeO_2 catalyst for CO_2 methanation was investigated.

2. Experimental

Ni (60wt%) supported on $Ce_{1-x}Zr_xO_2$ (x = 0 and 0.1) was prepared by an FSP reactor [1]. Appropriate amount of Ni (II) acetate tetrahydrate (Wako, purity > 98.0%), Zr 2-ethylhexanoate in mineral spirits (Wako, 11.7-12.3% as Zr) and Ce (III) 2-ethylhexanoate, 49% in 2-ethylhexanoic acid (Alfa Aesar, Ce: 12%) were mixed with a mixture (1: 1) of 2-ethylhexanoic acid (Sigma-Aldrich, purity > 99%): methanol (Wako, Reagent Grade) to be the total metal concentration (Ni + Zr + Ce) of 0.2 M. The precursor solution was fed to the two-fluid spray nozzle at 3 mL min^{-1}, dispersed to a fine spray by 5 L_{STP} min^{-1} of O_2 dispersant (technical grade). The spray was evaporated and combusted by a premixed CH_4/O_2 plot flame (1.5 L_{STP} min^{-1}/3.2 L_{STP} min^{-1}) to form particles. The particles were collected on a glass-fiber filter by a vacuum pump (Busch SV1040C). Also, 20 and 60 wt% of Ni was deposited on FSP-made pure CeO_2 by an impregnation method. Before the characterization and activity tests, all the catalysts were reduced in 5%H_2-Ar at 500°C for 1 h.

Catalytic activity was evaluated using a fixed bed reactor. The catalyst (100 mg) and SiC powder (400 mg) were filled into a quartz tube (inner/outer diameters of 6/8 mm). The catalyst was reduced at 500 °C for 1 h in 5% H_2–Ar (100 mL_{STP} min^{-1}), and subsequently, a reactant gas ($CO_2/H_2/N_2$ = 1/4/1) was fed to the catalyst at 60 mL_{STP} min^{-1}. The composition of the product was measured by a gas chromatograph equipped with a thermal conductivity detector.

3. Results and discussion

PXRD pattern of all the catalysts shows the peaks of fluorite CeO_2 at 28° and 33°. In the absence of Zr, the peak potions were identical while the Zr doping shifts the peaks to the higher diffraction angle. Additionally, the peaks of monoclinic and tetragonal ZrO_2 were not detected. These facts indicate the preferable Zr doping to the CeO_2 lattice. EDX mapping (not shown) exhibited the size of Ni in FSP-made 60Ni/CeO_2 and 60Ni/$Ce_{0.9}Zr_{0.1}O_2$ was small (10-20 nm), despite the high Ni content (60 wt%).

Figure 2 shows the activity of FSP-made and wet-made catalysts for CO_2 methanation. The conversion of FSP-made 60Ni/CeO_2 was higher than that of wet-made ones. Notably, the Zr doing by FSP significantly enhanced the catalytic activity. In addition, by-product (CO) was not detected for all the tests. In conclusion, highly active and selective catalyst was developed by simultaneously achieving high Ni content (60wt%), small Ni size (10-20 nm) and Zr doping to CeO_2 by FSP.

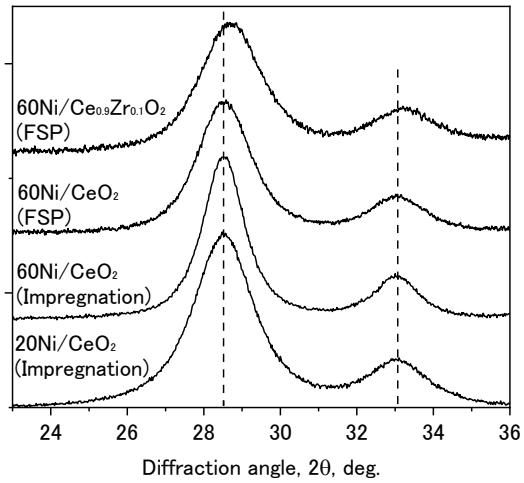

Fig. 1 PXRD patterns of FSP-made Ni/$Ce_{1-x}Zr_xO_2$ and wet-made Ni/CeO_2 particles

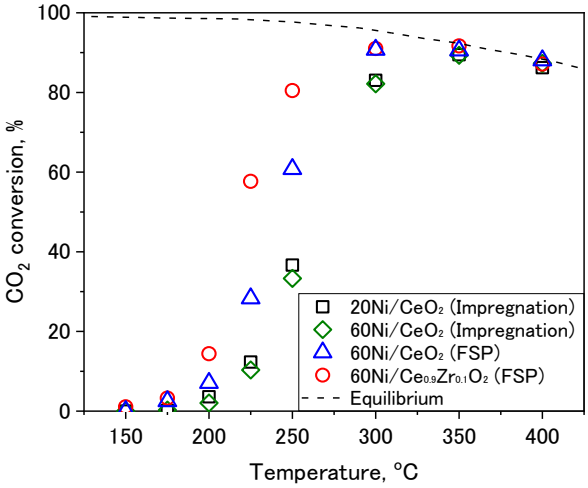

Fig. 2 Catalytic activity of FSP-made and wet-made catalysts for CO_2 methanation.

References

1. Fujiwara, K.; Tada, S.; Homma, T.; Sasaki, H.; Nishijima, M.; Kikuchi, R., AlChE *J.* **2019**, 65, e16717.

インターナショナル sess.

[2A01-02] インターナショナル sess.(4)

座長:霜田 直宏(徳島大学)

2021年11月12日(金) 09:00 〜 10:00 A会場 (函館アリーナ 会議室A)

[2A01] [Invited] Heterogeneous catalytic conversion of C1 gas to value-added chemicals

○Baek Jayeon[1] （1. Korea Institute of Industrial Technology (KITECH)）

09:00 〜 09:30

[2A02] 【招待】フェノールの酸化のためのマイクロポーラスチタノシリケート触媒の創製

○稲垣 怜史[1] （1. 横浜国立大学）

09:30 〜 10:00

Heterogeneous Catalytic Conversion of C1 Gas to Value-added Chemicals

(Korea Institute of Industrial Technology 1*) ○Jayeon Baek 1*

1. Introduction

Valorization of C1 gases including CO, CO_2, and CH_4 to useful chemicals is one of the carbon-neutral strategies and it supports a process of global consensus on climate change. This talk will cover three subjects of oxidative carbonylation of alcohols, CO_2 hydrogenation, and CH_4 selective oxidation using heterogeneous catalysts. The main target product from CO_2 hydrogenation and CH_4 selective oxidation is methanol and dialkyl carbonate through oxidative carbonylation of alcohol. These strategic developments are underway for practical applications.

2. Experimental

Metal−organic framework (MOF) based catalyst was used for the synthesis of methanol. Specifically, we reported a catalyst where Cu nanoparticle (NP) is encapsulated inside a Zr(IV)-based MOF denoted as Cu⊂UiO-66, UiO-66 [$Zr_6O_4(OH)_4(BDC)_6$, BDC = 1,4-benzenedicarboxylate], for CO_2 hydrogenation to methanol. For the methane oxidation to methanol, postsynthetic modification of MOF-808 [$Zr_6O_4(OH)_4(BTC)_2(HCOO)_5(H_2O)_1(OH)_1$, BTC = benzenetricarboxylate] was conducted where formate, water, or hydroxide molecules is replaced with imidazole-based ligand followed by Cu(I) insertion.

Se catalyst as well as tertiary amine base was utilized for the oxidative carbonylation of alcohol to methanol.

3. Results and Discussion

We show that the activity and selectivity of Cu catalyst can be promoted by a Zr-based MOF, UiO-66, to have a strong interaction with Zr oxide secondary building units (SBUs) of the MOF for CO_2 hydrogenation to methanol. These interesting features are achieved by a catalyst composed of 18 nm single Cu nanoparticle (NP) encapsulated within single crystal UiO-66 (Cu⊂UiO-66) (Fig.1). The performance of this catalyst construct exceeds the benchmark $Cu/ZnO/Al_2O_3$ catalyst and gives a steady 8-fold enhanced yield and 100% selectivity for methanol.

On the other hand, we show that, by selection of MOF with appropriate structure and topology, MOF-808 can be utilized as a scaffold to host and stabilize highly active copper−oxygen complexes, bis(μ-oxo) dicopper species, ligated to biologically relevant imidazole moieties including L-histidine (His), 4-imidazoleacrylic acid (Iza), and 5-benzimidazolecarboxylic acid (Bzz) inspired by pMMO. The catalysts show high selectivity for methane oxidation to methanol under isothermal condition at 150 °C (Fig.2).

Finally, we have developed the platform catalyst for the oxidative carbonylation of C1-C3 alcohols to corresponding dialkyl carbonate with the highest TOF value and also can replace corrosive Cu halide catalyst which is conventional catalyst (Fig.3). Especially, the synergistic effect between Se and base was revealed by density functional theory (DFT) calculations.

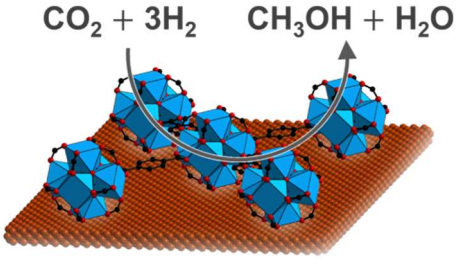

Fig.1. Selective hydrogenation of carbon dioxide to methanol via Cu nanoparticle encapsulated UiO-66.

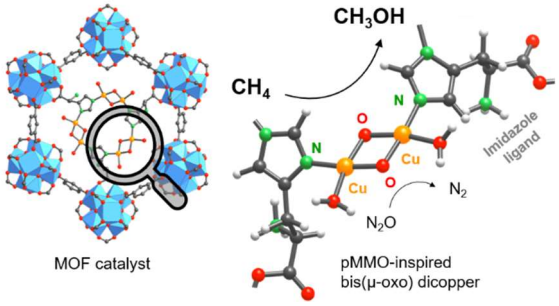

Fig.2. pMMO-inspired MOF catalyst to synthesize methanol from methane.

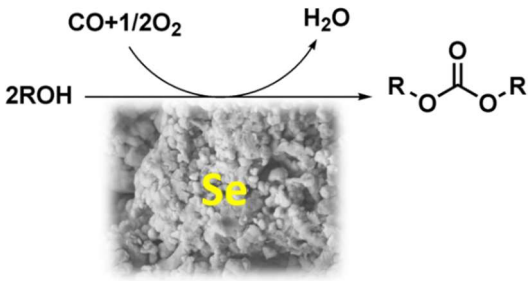

Fig.3. Oxidative carbonylation of alcohol to dialkyl carbonate through Se catalyst.

Development of microporous titanosilicate catalyst for the oxidation of phenol with H_2O_2

(YOKOHAMA National Univ.) Satoshi INAGAKI

1. Introduction

Titanosilicates with ordered microporosity are highly efficient catalysts for the selective oxidation of various organic substrates with H_2O_2 as an oxidant. It is well-known that titanium silicalite-1 (TS-1) with **MFI** topology (10-ring straight channel, 0.51 × 0.55 nm; 10-ring sinusoidal channel, 0.53 × 0.56 nm) is an industrially useful catalyst for the oxidation of phenol, the ammoximation of cyclohexanone, and the epoxidation of propylene.

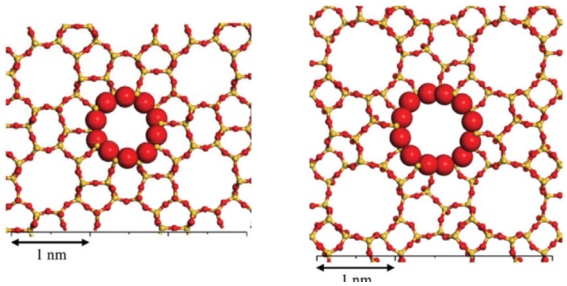

Figure 1. Projections of the (a) 10-ring window (0.51 × 0.55 nm) in TS-1 (**MFI** viewed along [010]) and (b) 12-ring window (0.64 × 0.68 nm) in Ti-MCM-68 (**MSE** viewed along [001]). The ionic radii of oxygen and silicon in the center of each figure are 0.135 and 0.04 nm, respectively.

Our group has proposed the preparation of [Ti]-MCM-68[1–4] and [Ti]-YNU-2[5–6], which consist of **MSE** topology (12-ring channel, 0.64 × 0.68 nm; 10-ring window, 0.52 × 0.58 nm), and their catalytic use in the oxidation of phenol. In this paper, it is reviewed that improving the hydrophobicity of titanosilicate catalysts gives rise to high catalytic activity and *para*-selectivity in the oxidation of phenol.

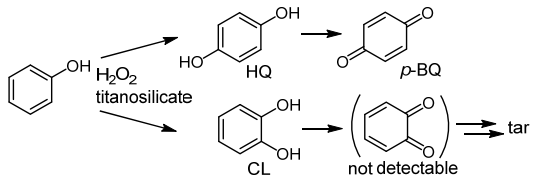

Scheme 1. The oxidation of phenol with H_2O_2.

2. Preparation of [Ti]-MCM-68[1)]

The synthesis of [Al]-MCM-68 was possible only under hydrothermal conditions using *N*,*N*,*N*′,*N*′-tetra ethylbicyclo[2.2.2]oct-7-ene-2,3:5,6-dipyrrolidinium diiodide, $TEBOP^{2+}(I^-)_2$, as the organic structure-directing agent (OSDA). The gel composition window for the successful crystallization of the pure [Al]-MCM-68 is very narrow, and the Si/Al ratio of the product is limited to the range of 9 to 12. In the case of the titanosilicate version, direct crystallization of [Ti]-**MSE** is still difficult. On the other hand, the two-step post-synthetic modification, dealumination by acid treatment followed by gas-phase Ti insertion using $TiCl_4$ as the Ti source, can be produced from [Al]-MCM-68 into [Ti]-MCM-68. The DR/UV-vis spectra of [Ti]-MCM-68 showed a sharp peak at ca. 210 nm (due to tetra-coordinated Ti) without any broad shoulder peaks at 250−290 nm (assignable to penta- and/or hexa-coordinated Ti). This means that most of Ti atoms can be incorporated into the **MSE** framework via $TiCl_4$ treatment.

In the oxidation of phenol (see Table 1), activity of the as-prepared [Ti]-MCM-68 was relatively lower than TS-1, but *para*-selectivity of the [Ti]-MCM-68 was prominent. The 12-ring of this catalyst should be suitable for the diffusion of a molecule of a single aromatic ring compound with the assistance of intersected 10-rings. It should be noted that the total yield in calcined [Ti]-MCM-68 was significantly greater than that in as-prepared Ti-MCM-68 and TS-1. Water adsorption isotherm measurements suggested that this improvement in catalytic activity was due to an increase in hydrophobicity (Figure 2).

Table 1. Oxidation of phenol with H_2O_2 over titanosilicates[a]

Catalyst	Si/Ti[b]	TON[c]	Yield (%)[d]				*p*-Sel.
			Total	HQ	CL	*p*-BQ	(%)[e]
[Ti]-MCM-68_as	62	111	13.9	8.2	5.3	0.4	62
[Ti]-MCM-68_cal	72	478	52.5	36.3	12.8	3.4	76
TS-1	44	140	24.3	12.7	10.4	1.1	57

a. Reaction conditions: catalyst, 20 mg; phenol, 21.25 mmol; H_2O_2, 4.25 mmol, H_2O, 17.9 mmol; temperature, 100°C; time, 10 min.
b. The Ti content per a gram-catalyst was determined by ICP-AES analysis.
c. Turnover number = moles of [HQ + CL + *p*-BQ] per mole of Ti site.
d. Product yields based on added H_2O_2.
e. Selectivity to *para*-isomers of dihydroxybenzenes and quinones (moles of [HQ + *p*-BQ] per moles of [HQ + CL + *p*-BQ]).

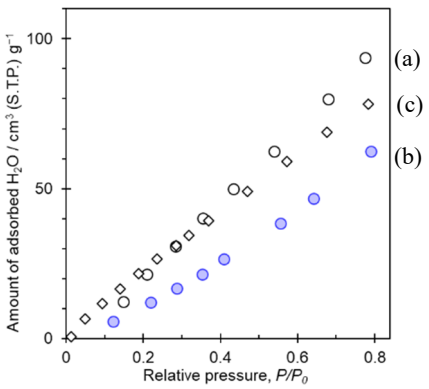

Figure 2. H_2O adsorption isotherms (25°C) of (a) [Ti]-MCM-68_as, (b) [Ti]-MCM-68_cal, and (c) TS-1.

3. Improvement of *para*-selectivity using the additive[2)]

Table 2 lists typical results for the oxidation of phenol over titanosilicate catalysts upon the addition of EtOH. The addition of EtOH in the [Ti]-MCM-68_cal system resulted in high total yield and *para*-selectivity. The hydrophobic [Ti]-MCM-68_cal containing only a trace amount of external Si–OH groups could interact with a lower amount of EtOH, resulting in a much more hydrophobic external surface, without pore narrowing, that helped guide phenol molecules into the 12-ring micropores and to allow shape-selective reactions to occur.

Table 2. Oxidation of phenol with H_2O_2 over titanosilicates[a]

Catalyst	Ti content (mmol/g)[b]	Additive	TON[c]	Yield (%)[d]				*p*-Sel. (%)[e]
				Total	HQ	CL	*p*-BQ	
[Ti]-MCM-68_as	0.235	neat	90	10.0	6.5	3.5	0.0	65.0
		EtOH	134	15.2	14.0	1.2	0.0	92.0
[Ti]-MCM-68_cal	0.241	neat	314	35.0	26.3	7.6	1.2	78.3
		EtOH	446	49.2	45.8	3.4	0.0	93.1
TS-1	0.373	neat	90	15.2	8.6	6.0	0.0	56.8
		EtOH	27	4.8	3.5	1.4	0.0	71.9

a. Reaction conditions: catalyst, 20 mg; phenol, 21.25 mmol; H_2O_2, 4.25 mmol, H_2O, 17.9 mmol, EtOH, 86.8 mmol; temperature, 70°C; time, 60 min.
b–e. as in Table 1.

4. Hydrothermal synthesis of (Ti,Al)-MCM-68[3)]

The first step in the synthesis of the Ti-containing **MSE**-type material is the preparation of the aluminosilicate gel containing titanium tetrabutoxide ($Ti(OBu^n)_4$) diluted with aqueous H_2O_2 solution. When the gel containing the Ti-source and H_2O_2 was statically heated in an autoclave at 160°C for 16 days, a white precipitate was obtained in high yield. After calcination at 650°C for the removal of occluded OSDA, the framework structure was retained with high crystallinity.

As confirmed by ICP-AES analysis, solid-state ^{27}Al MAS NMR spectroscopy, and UV-vis spectroscopy, both Al and Ti atoms were involved in the framework of the pristine sample, named (Ti, Al)-MCM-68.

It should be noted that the selective removal of Al from (Ti,Al)-MCM-68 occurred during the acid treatment, while most Ti species were intact. The UV-vis spectrum of (Ti)-MCM-68, which is selectively dealuminated sample, indicates that tetrahedral Ti species remain during the acid treatment, and there is no signal corresponding to extra-framework Ti species (240−260 nm).

Unfortunately, the catalytic activity of (Ti)-MCM-68 was as low as that of (Ti,Al)-MCM-68, probably due to their hydrophilic nature. Such hydrophilicity could be caused by silanol nests generated through dealumination from tetrahedral $Al(OSi)_4$ sites in the zeolite framework.

The (Ti)-MCM-68 calcined at 650°C is designated as (Ti)-MCM-68_cal, and it showed improved catalytic activity and selectivity, because of enhanced hydrophobicity.

Table 3. Oxidation of phenol with H_2O_2 over titanosilicates[a]

Catalyst	content (mmol/g)[b]		TON[c]	Yield (%)[d]				*p*-Sel. (%)[e]
	Ti	Al		Total	HQ	CL	*p*-BQ	
(Ti,Al)-MCM-68	0.16	1.34	56	4.2	0.8	2.8	0.6	33.3
(Ti)-MCM-68_as	0.15	<0.1	72	5.0	1.5	3.0	0.0	23.4
(Ti)-MCM-68_cal	0.15	<0.1	312	22.1	5.8	8.6	7.8	61.5

a. Reaction conditions: catalyst, 20 mg; phenol, 21.25 mmol; H_2O_2, 4.25 mmol, H_2O, 17.9 mmol, EtOH, 86.8 mmol; temperature, 70°C; time, 60 min.
b–e. as in Table 1.

5. Preparation of [Ti]-MCM-68 under mild conditions[4)]

The intense reactivity of $TiCl_4$ with moisture, even at room temperature, is a serious issue during this Ti insertion treatment. Therefore, a gentle Ti modification process in the liquid phase at room temperature is desirable. To introduce Ti into the site defects, commercially available "titanium(IV) chloride aqueous solution" was used as a reagent. This is a clear yellowish and viscous solution that was prepared by reacting $TiCl_4$ with excess water, and the analytical data were guaranteed as follows: Ti, 3.45 mmol g^{-1}; Cl, 8.18–9.32 mmol g^{-1}. The reaction of $TiCl_4$ with excess H_2O ideally gives a solution with a Cl/Ti molar ratio of 4; however, analytical data showed a lower value of Cl/Ti = 2.37–2.70, which indicates that some HCl was evaporated before the final solution was obtained. This aqueous solution, which is designated as Ti^{4+}/H_2O, consists of H^+, Cl^- and Ti^{4+} with various ligands such as H_2O.

Elemental analysis showed that a sufficient amount of Ti (0.20–0.22 mmol-Ti g^{-1}) was introduced into the dealuminated MCM-68 by treatment with the Ti^{4+}/H_2O at 25°C. In UV-visible spectroscopy, the as-prepared sample gave a clear peak at 210 nm, which corresponds to a tetra-coordinated Ti species at closed sites, $Ti(OSi)_4$, and a shoulder at 250 nm due to tetra-coordinated Ti species at open sites, $(OH)Ti(OSi)_3$, both of which are inside the framework. This reveals the successful incorporation of tetrahedral Ti into the silicate framework of dealuminated MCM-68 during the suitable treatment at room temperature.

Raman spectroscopy is one of the most informative techniques for evaluation of the coordination and conformation of Ti–ligand complexes. The Raman peaks of Ti^{4+}/H_2O (Fig. 3a) were entirely different from those of neat $TiCl_4$ (Fig. 3b) and $TiCl_4$/toluene (Fig. 3c). A broad band at 650 cm^{-1} and weak broad bands at 150, 340, 460, 790 and 934 cm^{-1} are assignable to $[Ti(OH_2)_6]^{4+}$ octahedra with considerable aggregation. It is reasonable to speculate that H_2O and framework oxygens behave as ligands for Ti^{4+}. The Ti^{4+} ions

diffuse into the 12-ring channels with repetitive ligand exchange to fill in a site defect of the silicate framework.

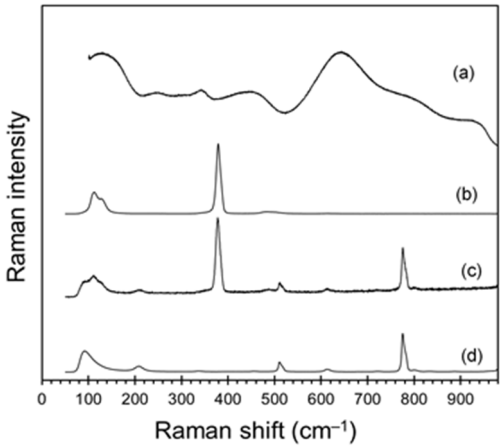

Figure 3. Raman spectra (532 nm laser) of (a) Ti^{4+}/H_2O, (b) neat $TiCl_4$, (c) $TiCl_4$/toluene, and (d) toluene.

[Ti]-MCM-68_Ti^{4+}/H_2O_as exhibited a meaningful product yield (11.4%) with subtle *para*-selectivity (61.2%). This behavior clearly shows the potential of the preparation methodology with mild treatment conditions using Ti^{4+}/H_2O at room temperature, and strongly supports the spectroscopic results suggesting the incorporation of 4-coordinated Ti species into the **MSE** framework with such a mild treatment. The reaction over Ti-MCM-68_Ti^{4+}/H_2O_cal obtained after thermal treatment at 650°C gave significantly enhanced total yield (88.9%) and *para*-selectivity (76.3%), due to improvement of the hydrophobicity.

Table 4. Oxidation of phenol with H_2O_2 over titanosilicates[a]

Catalyst	Ti content (mmol/g)[b]	TON[c]	Yield (%)[d]				*p*-Sel. (%)[e]
			Total	HQ	CL	*p*-BQ	
[Ti]-MCM-68 _Ti^{4+}/H_2O_as	0.206	12	11.4	5.1	4.4	1.8	61.2
[Ti]-MCM-68 _Ti^{4+}/H_2O_cal	0.214	832	88.9	58.9	21.0	9.0	76.3

a. Reaction conditions: catalyst, 20 mg; phenol, 21.25 mmol; H_2O_2, 4.25 mmol, H_2O, 17.9 mmol; temperature, 100°C; time, 60 min.
b–*e*. As in Table 1.

Acknowledgements

This work was financially supported in part by Grants-in-Aid for Scientific Research (no. 23760741, 15H04185 and 15K14221) from JSPS, and CONCERT-Japan (JPMJSC18C4) from JST. I am grateful to Professor Y. Kubota (YNU) and Honorary Professor T. Tatsumi (Tokyo Tech).

References

1) Y. Kubota *et al.*, *Chem. Commun.*, 6224 (2008).
2) S. Inagaki, *et al.*, *Green Chem.*, **18**, 735 (2016).
3) Y. Ikehara *et al.*, *Chem. Lett.*, **46**, 1842 (2017).
4) S. Inagaki *et al.*, *RSC Adv.*, **11**, 3681 (2021).
5) Y. Koyama *et al.*, *Angew. Chem. Int. Ed.*, **47**, 1042 (2008).
6) M. Sasaki *et al.*, *ACS Catal.*, **4**, 2653 (2014).

インターナショナル sess.

[2A03-05] インターナショナル sess.(5)

座長:田村 正純(大阪市立大学)

2021年11月12日(金) 10:15 ～ 11:00 A会場 (函館アリーナ 会議室A)

[2A03] オレフィンメタセシス重合のためのイミド配位ニオブ錯体の合成と触媒活性への配位子効果

○Chatchaipaiboon Kanchana[1]、野村 琴広[1] （1. 東京都立大学）

10:15 ～ 10:30

[2A04] Depolymerization of Lignin by Using Ionic Liquid and Ethylene Glycol

○Peng Mingming[1]、Nakabayashi Manaka[1]、Qian Eika[1] （1. Tokyo University of Agriculture and Technology）

10:30 ～ 10:45

[2A05] Aerobic oxidation of concentrated acetal-protected 5-HMF solutions to FDCA using nitrogen-doped carbon-supported cobalt as a non-noble metal catalyst

○Jan Wiesfeld[1], Atsushi Fukuoka[1], Kiyotaka Nakajima[1] （1. iCAT, Hokkaido University）

10:45 ～ 11:00

Imido(niobium) Complexes Catalysts for Olefin Metathesis Polymerization

(都立大院理) ○Kanchana Chatchaipaiboon and Kotohiro Nomura*

1. Introduction

Ring opening metathesis polymerization (ROMP) has been widely used in synthesis of advanced materials, and high oxidation state early transition metal carbene (alkylidene) complexes play an essential role as catalyst. Development of the niobium catalysts has been an attractive subject due to a promising possibility, however, reported examples have been limited such as metallacycle (**A**, **Scheme 1)**, dialkyl complex containing chelate ligand (**B**) and alkyl, alkylidene complex (**C**). Noteworthy, only imido-alkylidene complex (**1**) exhibited promising catalytic performances and proceed in a living manner.[1] We thus explored more details to develop the alkylidene complexes for the catalyst not only for ROMP of norbornene (NBE), but also for low strain monomers.

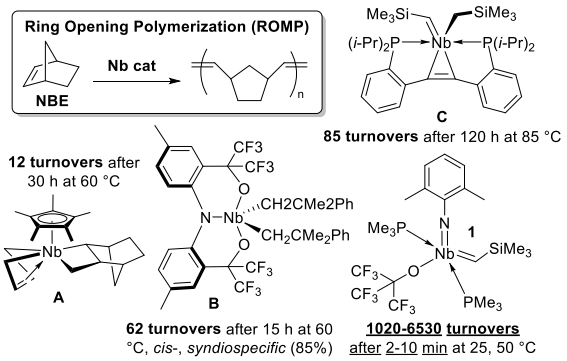

Scheme 1

2. Experimental

All experiments were carried out under nitrogen atmosphere in the drybox. Molecular weights and the molecular weight distributions in the resulting polymers were measured by GPC.

3. Results and discussion

The alkoxy alkylidene complexes, Nb(CHSiMe$_3$)-(NAr)[OC(CF$_3$)$_3$](PMe$_3$)$_2$, [Ar = 2,6-Me$_2$C$_6$H$_3$ (**1**), 2-MeC$_6$H$_4$ (**2**), 2,6-Cl$_2$C$_6$H$_3$ (**3**), 2,6-F$_2$C$_6$H$_3$ (**4**)] and the phenoxy analogue, Nb(CHSiMe$_3$)(N-2,6-Cl$_2$C$_6$H$_3$)-(OC$_6$F$_5$)(PMe$_3$)$_2$ (**5**) could be isolated from the dialkyl complexes by α-hydrogen elimination upon heating in *n*-hexane in the presence of excess PMe$_3$ (**Scheme 2**). All complexes were fully characterized by NMR spectra and elemental analysis. The results for ROMP of NBE in toluene are summarized in **Table 1**.

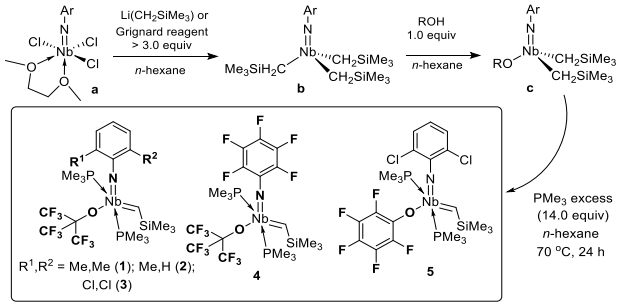

Scheme 2

Complexes **1-5** exhibited remarkable activities for ROMP of NBE at 25 °C and activities increased at high temperature, clearly suggesting that the activity can be tuned by the ligand modification of imido and anionic donor ligands. Note that **4** and **5** exhibited rather high activities and reached completion even under low catalyst loading at 50 °C. Moreover, activities in ROMPs of NBE derivatives by alkoxy analogues (**1-3**) were higher than those in the ROMPs of NBE.[2] Also note that these Nb-alkylidene complexes enable ROMP of low strain monomers as the first demonstration by Nb. More details will be introduced in the symposium.

Table 1. ROMPs of NBE by **1-5**. [a]

cat. (μmol)	temp / °C	time / min	yield / %	TOF[b] / sec^{-1}	M_n[c] ×10^{-5}	M_w /M_n[c]	*cis*[d] / %
1 (0.3)	25	5	66	15.5	15.3	1.14	70
2 (0.3)	25	5	49	11.6	6.90	2.09	56
3 (0.3)	25	5	51	12.0	6.47	2.14	--
4 (0.2)	25	5	83	29.2	7.38	2.46	59
5 (0.2)	25	5	95	33.7	8.88	2.72	47
1 (0.3)	50	2	90	52.9	60.9	1.61	--
2 (0.5)	50	2	91	32.0	7.59	2.14	58
3 (0.5)	50	2	88	31.2	10.4	2.02	68
4 (0.2)	50	0.5	>99	353	8.25	2.78	62
5 (0.2)	50	0.5	>99	353	15.3	2.48	48

[a] Conditions: toluene 4.8 mL, NBE 2.12 mmol (initial monomer conc. 0.44 mmol/mL). [b]TOF = TON/time. [c]GPC data in THF vs polystyrene standards. [d]Estimated by ^{1}H NMR speatra.

References

(1) (a) K. Wised, K. Nomura, *Organometallics*, **2016**, *35*, 2773-2777. (b) Izawa, I.; Nomura, K. *Macromolecules*, **2020**, *53*, 5266.
(2) Chatchaipaiboon, K.; Nomura, K. *J. Jpn. Petrol. Inst.*, **2021**, *64(5)*, 238-244.

Depolymerization of Lignin by Using Ionic Liquid and Ethylene Glycol

(Tokyo University of Agriculture and Technology) ○Mingming Peng, Manaka Nakabayashi, Eika. W. Qian

1. Introduction

Lignin, as an important component in lignocellulosic biomass, has been considered as a potentially renewable carbon resource due to its polyphenolic structure.[1] The hydrothermal liquefaction of lignin into production of high-value aromatics, i.e., phenol, benzene, toluene, xylene, vanillin, etc., is a very promising way to sustainable utilization of lignin. Ionic liquids (ILs) as novel medium showed many unique characteristics, like hydrophilicity/hydrophobicity, solvation power, etc. It provided a very useful solution for the products extraction and low energy separation after the reaction. Ethylene glycol (EG) as an alcoholic solvent gives a very good solubility for lignin, but also it is very vital to improve the aromatics yield as a stabilization agent. In this study, the catalytic depolymerization for lignin and lignin model compounds by using the synergic catalysis of [Apy]OH-NaCl in EG and ILs co-solvents were developed on a continuous flow fixed-bed reactor.

2. Experimental section

Lignin model compounds were purchased from Tokyo Chemical Industries. Ionic liquids N-allylpyridinium chloride ([APy]Cl) was synthesized according to our previously described methods.[2,3] The depolymerization of lignin and lignin model compounds were carried out in a continuous flow fixed-bed reactor. Five kinds of substances, lignin or lignin model compounds, ILs, NaOH, H_2O, and EG with different mass ratio, were premixed at room temperature. The flow rate was set at 2.5 ml/h. The reactor temperature was 180 ℃. The unreacted lignin after the reaction was precipitated by acetonitrile, and the liquid products were extracted by ether after adjusting the pH value to 2, and analyzed by GC-FID and GC-MS.

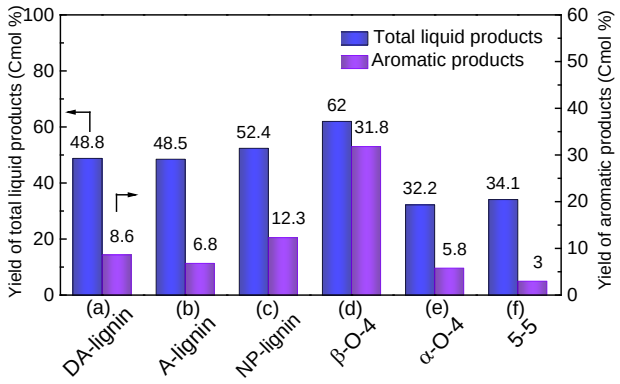

Figure 1. Catalytic depolymerization results of different categories of lignin and lignin model compounds. Reaction conditions: Temp. 180 ℃; flow rate, 2.5 ml/h.

3. Results and discussion

Figure 1 showed the reaction results of lignin and lignin model compounds depolymerization. The liquid products contained monoaromatics and other aliphatic compounds. The main aromatic products included 4-methyl-benzaldehyde, guaiacol, and 3-Methylbenzyl alcohol, etc. NP-lignin (sodium lignosulfonate) present the highest yields of liquid products and aromatic compounds in all lignin. DA-lignin (dealkaline lignin) and A-lignin (alkaline lignin) both obtain similar results, regardless of the presence or absence of sodium ions. β-O-4 model compound presented a higher aromatic yield than α-O-4 and 5-5, which proved the C-O bond was easily cracked in the reaction condition. Most of aromatic products in lignin depolymerization probably came from the cracking of β-O-4 linkage.

1) Zakzeski J., Bruijnincx P. C. A., Jongerius A. L., Weckhuysen B. M., *Chem. Rev.*, **110**, 3552 (2010).
2) Wang X., Wang N., Nguyen T. T., Qian E. W., *Ind. Eng. Chem. Res.* **57**, 49, 16995 (2018).
3) Wang X., Luo Y., Qian M., Qian E.W., *Sustainable Energy Fuels*, **4**, 1409 (2020).

Aerobic oxidation of concentrated acetal-protected 5-HMF solutions to FDCA using nitrogen-doped carbon-supported cobalt as a non-noble metal catalyst.

(Hokkaido Univ.) ○ Jan Wiesfeld, Atsushi Fukuoka, Kiyotaka Nakajima*

1. Introduction

The copolymer of bio-based FDCA and ethylene glycol (polyethylene furanoate, PEF) is recognized as a replacement for polyethylene terephthalate (PET). Recently, our group reported the production of FDCA in high yield (>92%) from concentrated solutions (>10 wt%) of HMF protected as its acetal with 1,3-propanediol (HMF-acetal) using a supported noble metal (gold) catalyst.[1] Here, we examined nitrogen-doped carbon-supported cobalt catalyst (Co@C-N) in a three-step approach (Fig. 1) that offers high FDCA yield and high PDO recovery in concentrated solutions.[2]

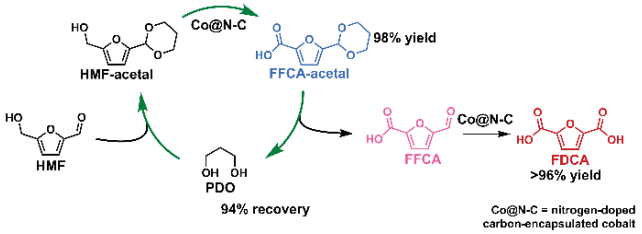

Fig. 1. Schematic representation of three-step approach.

2. Experimental method

Nitrogen-doped carbon encapsulated cobalt catalyst (Co@N-C) was prepared via pyrolysis of ZIF-67 precursor analogous to procedures described in literature.[2,3] HMF-acetal and FFCA-acetal were prepared as described in earlier works.[1] All oxidation reactions were performed in 10 mL steel batch reactors with PTFE liners. Reactors were loaded with 100 mg substrate, 100 mg Co@N-C, 2 mol. eq. Na_2CO_3 and 1 mL H_2O, pressurized with 2 MPa air, and then heated to 100 °C for a specified duration. Reaction mixtures were analyzed by HPLC using an Aminex HPX-87H column and 5 mM H_2SO_4 as mobile phase.

3. Results and discussion

Pyrolysis of ZIF-67 yielded Co@N-C containing ~37 wt% Co in both metallic and oxidic states, with an average particle size of 15 nm estimated by Scherrer equation. Kinetic data in Fig. 2 shows that stepwise oxidation of HMF-acetal proceeds selectively to DFF-acetal (k_1 = 2.7 h^{-1}) and FFCA-acetal (k_2 = 2.5 h^{-1}), together with the formation of FDCA in only very minor quantities (k_3 = 0.007 h^{-1}). This is due to the alkaline reaction medium in which the acetal does not hydrolyze, which prevents further oxidation to FDCA and byproduct formation from the reactive formyl groups in non-protected HMF, DFF, and FFCA.

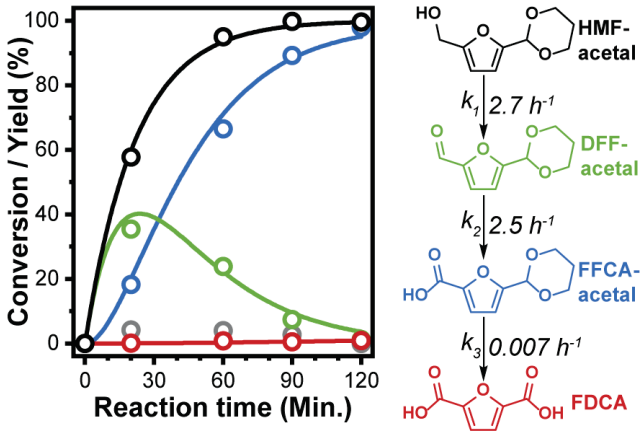

Fig. 2. Time-course plots of HMF-acetal oxidation over Co@C-N.

Deprotection of the so-formed FFCA-acetal can be performed in acidic water (pH 1), yielding FFCA and PDO in > 99.5% yields after heating the mixture at 65 °C for 4 hours (Fig 3b). Co@N-C was also effective for the oxidation of FFCA using a 10 wt% solution under similar conditions, producing FDCA in 96% yield (Fig 3c).

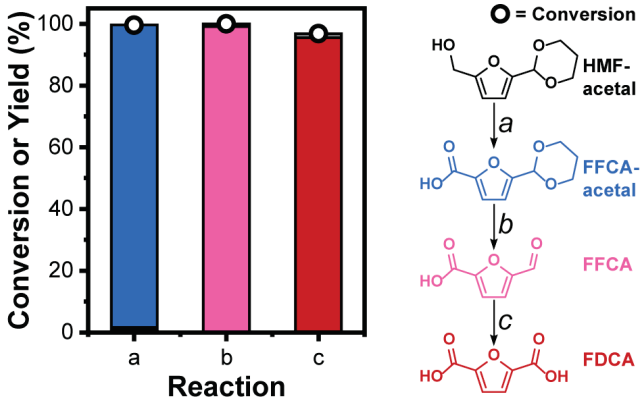

Fig. 3. Three-step approach using Co@C-N: (a) oxidation of HMF-acetal to FFCA-acetal, (b) deprotection of FFCA-acetal to FFCA, and (c) oxidation of FFCA to FDCA.

References

(1) Kim, M. et al., Angew. Chem. Int. Ed. 2018, 57 (27), 8235–8239.
(2) Zhong, W. et al., ACS Catal. 2015, 5 (3), 1850–1856.
(3) Qian, J. et al., Mater. Lett. 2012, 82 (2012), 220–223.

インターナショナル sess.

[2A06-08] インターナショナル sess.(6)

座長:吉田 暁弘(弘前大学)

2021年11月12日(金) 11:15 〜 12:00 A会場 (函館アリーナ 会議室A)

[2A06] Sugars dehydration with Nb-based mixed metal oxide catalysts

○Daniele Padovan[1], Hideki Kato[2], Atsushi Fukuoka[1], Kiyotaka Nakajima[1] （1. Institute for Catalysis, Hokkaido University, 2. Institute of Multidisciplinary Research for Advanced Materials, Tohoku University）

11:15 〜 11:30

[2A07] イオン性液体溶媒中での非環式ジエンメタセシス重合によるバイオベースポリエステルの合成

○王 秀々[1]、Zhao Weizhen[2]、野村 琴広[1] （1. 東京都立大学、2. 中国科学院　過程工程研究所）

11:30 〜 11:45

[2A08] Reductive amination of 5-formyl-2-furancarboxylic acid to 5-(aminomethyl)furan-2-carboxylic acid

○Tat Boonyakarn[1], Jan J Wiesfeld[1], Atsushi Fukuoka[1], Takato Mitsudome[2], Kiyotaka Nakajima[1,3] （1. Institute for Catalysis, Hokkaido University, 2. Department of Materials Engineering Science, Graduate School of Engineering Science, Osaka University, 3. JST-MIRAI）

11:45 〜 12:00

Sugars dehydration with Nb-based mixed metal oxide catalysts.

([1]ICAT, Hokkaido Univ.; [2]IMRAM, Tohoku Univ.; [3]JST·MIRAI)

○Daniele Padovan[1] · Hideki Kato[2] · Atsushi Fukuoka[1] · Kiyotaka Nakajima[1,3,*]

In this work we explore the utility of a mixed oxide, $YNbO_4$, for the selective dehydration of glucose into 5-hydroxymethylfurfural (HMF), an important key intermediate for biomass-based commodity chemicals. Precise control on Lewis acidity and basicity with phosphoric acid modification improved the overall characteristics of the $YNbO_4$ catalyst.

Solid Lewis acid, Heterogeneous catalysis, Biomass

nakajima@cat.hokudai.ac.jp (Kiyotaka Nakajima)

1. Introduction

Glucose is the most abundant sugar in nature and can be obtained by the hydrolysis of non-edible cellulose. Dehydration of glucose produces HMF that is an important key intermediate for biorefinery processes (Fig. 1). Phosphate/Nb_2O_5 can catalyze sugar dehydration in water *via* stepwise dehydration mechanism by water-tolerant Lewis acid sites.[1,2)] Introduction of the base character can control intrinsic Lewis acidity of Nb_2O_5, which is beneficial for the development of highly active Nb-based catalysts. Recently, $YNbO_4$ has been found to possess Lewis acid-base pairs that convert glucose to lactic acid in water.[3)] In this work we apply this material to the synthesis of HMF. Phosphoric acid impregnation on the catalyst was successfully used to tune the acid-base properties of the material.

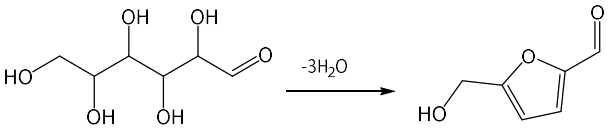

Fig. 1 Synthesis of HMF *via* glucose dehydration.

2. Experimental method

YNbO4 was prepare by a co-precipitation method, followed by calcination at 700°C.[3)] Phosphoric acid was impregnated at 150°C to obtain xP-$YNbO_4$, where x represents the number of phosphate groups per nm^2 of surface area. The catalytic reaction was performed in a pressure-resistant glass tube placed inside a thermostated oil bath. Typically, a mixture ofH2O (2 mL), 3 wt.% glucose (60 mg), NaCl (240 mg), catalyst (100 mg), and methyl tetrahydropyran (MTHP, 7 mL) was heated at designated temperatures for various times. After the reactions, aliquots were analyzed by HPLC.

3. Result and Discussion

$YNbO_4$ was impregnated with different amount of phosphate groups and tested for HMF formation (Fig. 2).

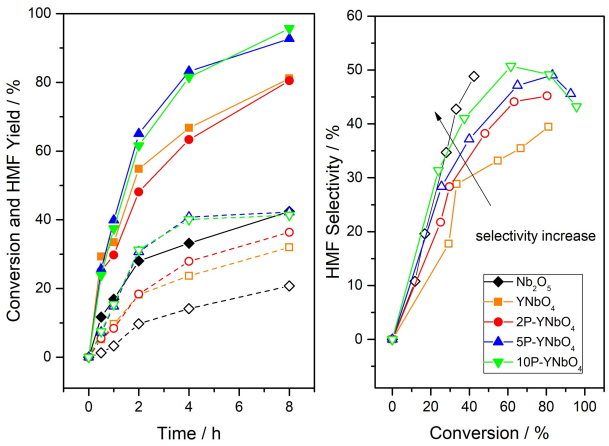

Fig. 2 Kinetics of glucose dehydration to HMF with $YNbO_4$, 2P-, 5P-, 10P-$YNbO_4$ and Nb_2O_5 catalyst.

Increasing the amount of phosphate groups positively impact both activity and selectivity. In particular, optimized 5P-$YNbO_4$ displayed a 4-fold increase of activity compared to the reference Nb_2O_5, maintaining the same level of HMF selectivity (~45-50%). $YNbO_4$ is significantly less selective compared to 5P-$YNbO_4$ (35 vs 50 %). In order to understand to role of basic sites and phosphate groups, several characterization techniques were used. ^{31}P solid-state MAS NMR showed that phosphorous was present uniquely as phosphate group esterified on the catalyst surface. However, IR analysis of pyridine-adsorbed samples showed that only Lewis acids were present and no Brønsted acids were identified, even in the presence of phosphate groups. Interestingly, $CHCl_3$-IR experiment showed that acid-base pairs present in the original $YNbO_4$ disappeared after phosphate impregnation, leading to a purely Lewis acid $YNbO_4$ material. Finally, CO_2-TPD showed total loss of basic character on P-$YNbO_4$, while NH_3-TPD showed an increase in the acid density and strength. Therefore, we conclude that introduction of phosphate groups on $YNbO_4$ likely suppresses base-promoted side reactions, increasing the HMF selectivity, and enhances the activity by increasing the acid strength and density of the Nb-derived Lewis acid centers.

References

1) K. Nakajima *et al.*, *JACS*, **133**, 133 (2011)

2) N. K. Gupta *et al.*, *ACS Catal.*, **7**, 2430 (2017)

3) M. Kim *et al.*, *ChemCatChem*, **12**, 350 (2020)

Synthesis of Bio-based Polyesters by Acyclic Diene Metathesis (ADMET) Polymerization in Ionic Liquid

(都立大院理*・中科院過程工程研**) ○Xiuxiu Wang*・Weizhen Zhao**・Kotohiro Nomura*

1. Introduction

Synthesis of bio-based polyesters attracts considerable attention due to utilization of abundant feedstocks as alternative of fossil fuels, as well as tunable mechanical properties and potential biodegradability in the resultant polymers.[1] The acyclic diene metathesis (ADMET) polymerization with Ru catalysts, $RuCl_2(IMesH_2)(CH\text{-}2\text{-}O^iPr\text{-}C_6H_4)$ (**HG2**) generally gave rather high molecular weight unsaturated polyesters, but repetitive removal of ethylene, accompanied by-product in this condensation polymerization, was prerequisite.[2-4] Unlike organic solvents, use of ionic liquids (ILs) plays an important role as solvent to remove ethylene and dissolve the resultant polymers due to extremely low vapor pressure, high boiling point and the good dissolving ability. We herein present that synthesis of the high molecular weight polymers can be simply achieved by conducting the ADMET polymerization in ILs as solvent (Scheme 1).

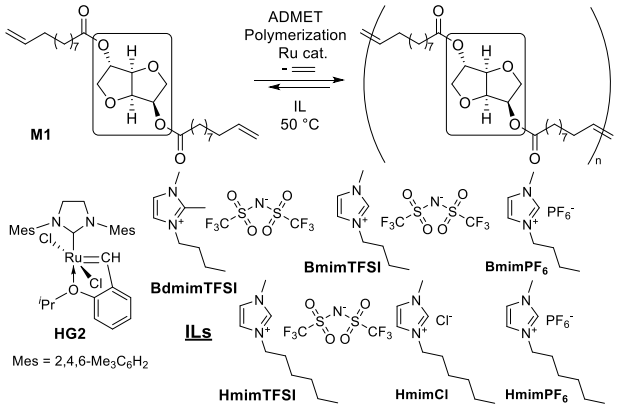

Scheme 1

2. Experimental

The ADMET polymerizations of dianhydro-*D*-glucityl bis(undec-10-enoate) (**M1**) by **HG2** catalyst were conducted in ILs *in vacuo*. Molecular weights and molecular weight distributions for the resultant polymers were measured by GPC, and their microstructure was analyzed by ^{1}H NMR spectra.

3. Results and discussion

The results in ADMET polymerization of **M1** by **HG2** in a series of ILs are summarized in Table 1. It was found that these polymerizations afforded high molecular weight polymers with unimodal molecular weight distributions. The M_n value increased slightly after 6 h and the catalyst was stable under these conditions. Note that the polymerizations conducted in **BmimPF$_6$** and **HmimTFSI** afforded higher molecular weight polymers than those conducted in the others, suggesting that the M_n value was affected by kind of the ILs employed. Various ILs with different alkyl chain length and counter anions were thus employed and more details will be introduced in the symposium.

Table 1. ADMET polymerization of monomer (**M1**) with **HG2** catalyst in ionic liquids (ILs).[a]

IL	time / h	yield[b] / %	M_n[c]	M_w/M_n[c]
BmimPF$_6$	6	87	24700	1.97
BmimPF$_6$	16	89	32200	1.87
BmimTFSI	6	86	17700	1.79
BmimTFSI	16	93	23000	1.94
BdmimTFSI	6	87	20000	1.73
BdmimTFSI	16	92	23600	1.88
HmimCl	6	84	6100	1.74
HmimCl	16	91	11200	1.65
HmimPF$_6$	6	87	11600	2.15
HmimPF$_6$	16	89	19100	1.69
HmimTFSI	6	89	28600	1.76
HmimTFSI	16	93	39200	1.95

[a]Conditions: HG2 1.0 mol%, monomer 300 mg in IL 0.14 mL (initial M1 conc. 4.64 M), 50 ºC *in vacuo*. [b]Isolated yield as MeOH insoluble fraction. [c]GPC data in THF vs polystyrene standards.

References

(1) K. Nomura, N. W. B. Awang, *ACS Sustainable Chem. Eng*., **9**, 5486 (2021).

(2) D. Le, C. Samart, S. Kongparakul, K. Nomura, *RSC Adv*. **9**, 10245 (2019).

(3) K. Nomura, P. Chaijaroen, M.M. Abdellatif, *ACS Omega*, **5**, 18301 (2020).

(4) M. Kojima, M. M. Abdellatif, K. Nomura *Catalysts*, **11**, 1098 (2021).

Reductive amination of 5-formyl-2-furancarboxylic acid to 5-(aminomethyl)furan-2-carboxylic acid

(Hokkaido Univ.,[1*] Osaka Univ.,[2**] JST·MIRAI[3**]) ○Tat Boonyakarn[1*], Jan J. Wiesfeld[1*], Atsushi Fukuoka[1*], Takato Mitsudome[2**], Kiyotaka Nakajima[1*,3**]

1. INTRODUCTION

5-(Aminomethyl)furan-2-carboxylic acid (AMFCA) is a potential monomer for the production of biobased aromatic or semi-aromatic polyamides. Biomass-derived 5-formyl-2-furan carboxylic acid (FFCA) can be converted to AMFCA via reductive amination as shown in Fig. 1, but no promising strategy has been developed so far. In this study we have studied reductive amination of FFCA using stable and highly active heterogeneous catalyst.

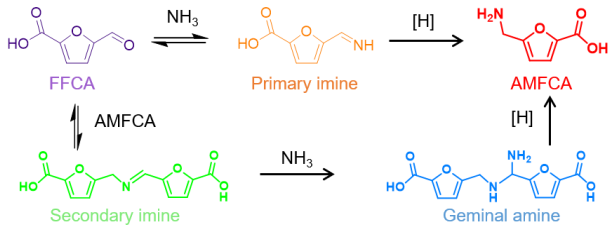

Fig. 1 Reaction pathways for the conversion of FFCA to AMFCA by reductive amination through primary imine and secondary imine.

Recently, cobalt phosphide nanorod (Co_2P) catalyst containing coordinatively unsaturated Co–Co active sites was reported as a new class of air-stable, highly active, and reusable heterogeneous catalysts for the reductive amination of carbonyl compounds to their corresponding primary amines using NH_3 or NH_4OAc as green amination reagents.[1,2] The air stability and high activity of the Co_2P is noteworthy, as conventional Co catalysts are air-sensitive (pyrophoric) and show very limited activity for this transformation under mild reaction conditions.[1,2] We have applied the Co_2P catalyst to reductive amination of FFCA to AMFCA.

2. EXPERIMENTAL

Co_2P was prepared according to literature.[2] Catalytic reactions were performed in Teflon lined batch reactors. Reactors were loaded with 0.5 mmol of FFCA, 5 mmol NH_4OAc, 0.03 mmol Co_2P, 2 mL MeOH, and 1 mL H_2O, then pressurized with 0.5 MPa H_2 and heated to 120°C for a pre-set duration. Reaction mixtures were analyzed by HPLC using an Shodex ODP2 HP-4E column and mobile phase using phosphate buffer (pH10) 23% and MeCN 77%.

3. RESULTS AND DISCUSSION

Reductive amination of FFCA in water in the presence of NH_3 or NH_4OAc produces undetectable byproducts always in 30-50% selectivity. However, such byproducts formation was found to be suppressed largely in a methanol-water (2:1 v/v) mixture using NH_4OAc as shown in Fig. 2. In this reaction system, FFCA was present in the mixture of bare form and dimethylacetal form (FFCA-acetal). FFCA and FFCA-acetal decreased with time and finally disappeared (~0%) at 180 min. The product found after 30 min was the secondary imine formed from FFCA and AMFCA (Fig 1). Free AMFCA was detected after 60 minutes, together with a decline in secondary imine. Maximum AMFCA yield was 95% at full conversion, together with minor byproducts including as 5-(hydroxymethyl)-2-furan carboxylic acid (HMFCA) in only 5%. AMFCA formed at the initial stage via primary imine is consumed for the formation of secondary imine, as shown in Figure 1. Low yield of secondary imine and steep increase in AMFCA yield after secondary imine formation suggested that primary imine pathway is slow compared to secondary imine pathway. Increase in AMFCA concentration promoted secondary imine, which leads to more efficient production of AMFCA.

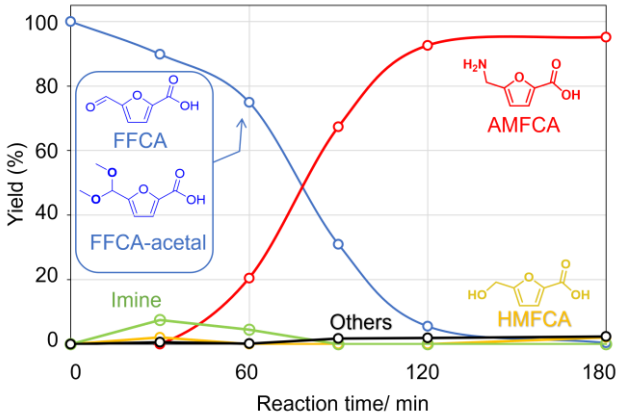

Fig. 2 Time course for reductive amination of FFCA in methanol-water mixture using NH_4OAc; AMFCA yield (red), FFCA and FFCA-acetal yield (blue), imine yield (green), and others (black).

(1) Mitsudome, T. *et al.*, *Chem. Sci.* **2020**, *11* (26), 6682–6689.
(2) Sheng, M. *et al.*, *JACS Au* **2021**, *1* (4), 501–507.

インターナショナル sess.

[2A09-10] インターナショナル sess.(7)

座長:大山 順也(熊本大学)

2021年11月12日(金) 13:30 〜 14:30 A会場 (函館アリーナ 会議室A)

[2A09] [Invited] Computational studies on atomic layer deposition mechanisms of Al_2O_3

○Kim Ki-Chul[1] （1. Konkuk University）

13:30 〜 14:00

[2A10] 【招待】ハイスループット実験を基盤としたデータ駆動型触媒探索

○谷池 俊明[1] （1. 北陸先端科学技術大学院大学 先端科学技術研究科）

14:00 〜 14:30

Computational studies on atomic layer deposition mechanisms of Al2O3

(Konkuk University, Korea) Ki Chul Kim*

1. Introduction

Atomic layer deposition (ALD) has been a popular technique for efficiently depositing thin films of various materials with precise growth control for a variety of applications, such as semiconductor devices, lithium-ion batteries, fuel cells, and solar cells. Most studies highlight how the ALD technique can be commonly applied to a broad array of applications. These studies also emphasize that understanding the fundamental chemistry of the ALD processes would be needed to optimize the performance of the ALD-prepared thin films. In this presentation, we employ the DFT modeling approach to explore the chemisorption behaviors of TMA molecules on the active adsorption sites of the Al2O3 surfaces and to investigate the possibility of the dimeric adsorption of TMA during the TMA-dosed half-cycle. The thermodynamic characteristics associated with the subsequent H2O-dosed half-cycle are further investigated to understand the ALD chemistry.

2. Computational Methods

All the DFT calculations were performed using the Quantum Espresso package with Perdew–Burke–Ernzerhof (PBE) generalized gradient approximation functional. The core electrons of each atom were described by ultrasoft pseudopotential. Energy cutoffs for wave function (680 eV) and charge density (6530 eV) were confirmed to be large enough to reliably predict the electronic structures. The bulk structure of the Al2O3 structure was geometrically optimized, allowing supercell and all atoms in the cell to fully relax until the forces on all atoms were less than 0.01 eV/Å. The Al2O3(0001) surface model was further developed through the cleavage of the optimized bulk structure followed by the hydroxylation of the surface dangling bonds. Note that the Al2O3(0001) surface was selected because the surface was the most stable in the thermodynamic point of view, exhibiting the lowest surface energy among possible low Miller index surfaces. The surface optimization was performed via the same procedure as the bulk optimization, except fixing the supercell. The resultant surface model contains six Al–O layers with a vacuum thickness of 30 Å. Such a large vacuum thickness would prevent the interaction between neighboring slab images, leading to the negligible effect of the dipole moment in the surface model.

3. Results and Discussion

We successfully identified the most stable formation for TMA chemisorption on the hydroxylated Al2O3 surfaces. As shown in Figure 1, in general, bidentate configurations are predicted to be more stable than monodentate configurations owing to the higher connectivity between Al and surface O atoms for the former. It is also unambiguous to see that the TMA species on the surface would thermodynamically prefer to be chemisorbed in a monomeric form rather than in a dimeric form. The formation energies for four MS-based models (MS2–MS5) are predicted to be ranged within −3.39 to −4.81 eV/2 TMA, which would be more negative than the values (−2.41 and – 2.89 eV/2 TMA) for DS-based models. It is further noted that the bond lengths (2.1 Å) of Al and C binding two monomeric species in the DS models are greater by 0.2 Å than the other Al–C bond lengths in the MS and DS models. Considering the relative thermodynamic stability of the models in terms of the bond geometry, the presence of a TMA molecule weakly maintained by these loose bonds for each DS model would be a critical indicator to describe the characteristics of the DS models less stable than the MS models.

The most striking observation from Figure 2 is that the energy profile for the sequential chemisorption of water molecules strongly relies on the configuration of TMA adsorbates on the surface at the early stage of the H2O-dosed half-cycle. The chemisorption of water molecules on the TMA (MS2)-chemisorbed surface exhibits a constant energy profile within the range of −1.32 to −1.35 eV/H2O, regardless of the number of chemisorbed water molecules (i.e., the number of the hydroxylation events in the sequential chemisorption of water). Considering that all the TMA species are uniformly chemisorbed on the bare surface in a bidentate configuration, all the active adsorption sites (monomethylaluminum groups) for the subsequent chemisorption of water molecules would be identical in the thermodynamic point of view. In addition, the space between neighboring TMA adsorbates is large enough to neglect the self-interaction between the water molecules chemisorbed on the neighboring TMA adsorbates. The constant energy profile for the TMA (MS2)-chemisorbed surface can be reasonably explained from all this evidence. In contrast to the MS2

configuration, the active adsorption sites for the chemisorption of water molecules on the TMA (MS3)-chemisorbed surface are not identical due to the co-existence of monodentate and bidentate configurations.

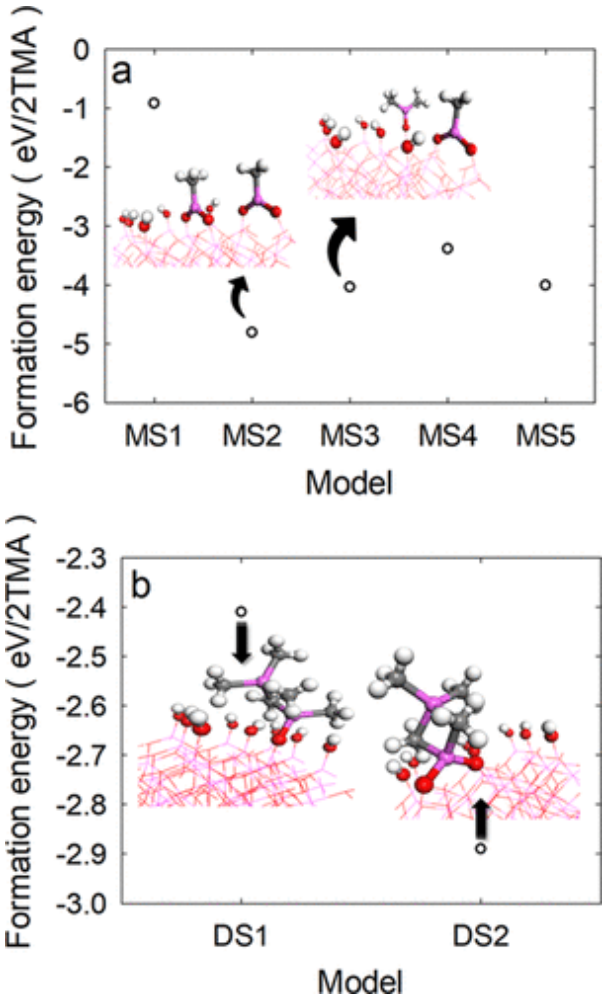

Figure 1. Thermodynamics of MS and DS. The DFT-calculated total energies of (a) five MS and (b) two DS models.

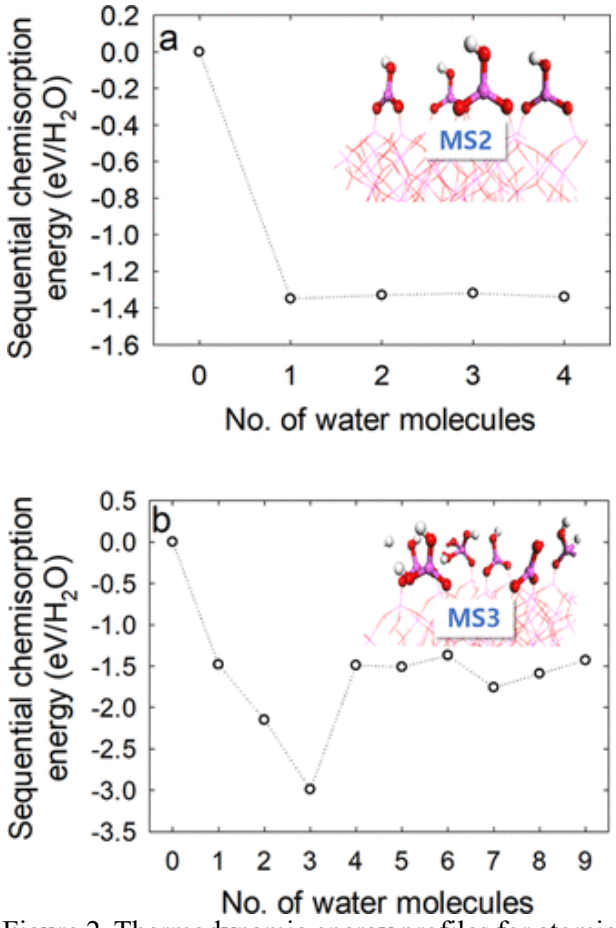

Figure 2. Thermodynamic energy profiles for atomic layer deposition processes. The change in the DFT-calculated sequential chemisorption energy during the water-based atomic layer deposition cycle for (a) MS2 and (b) MS3 models.

Data-driven catalyst discoveries based on high-throughput experimentation

(Japan Advanced Institute of Science and Technology) ○Toshiaki Taniike

Materials informatics (MI) is a data scientific approach to materials science, and its use has been extensively attempted in almost all fields of materials science. The application of data science premises the existence of a dataset sufficient in terms of size, distribution, and consistency. In particular, given that many machine learning methods prioritize data points with a relatively large number and enable prediction mainly via interpolation, the data points must be uniformly sampled over the entire parameter space to be explored. One of the biggest challenges in MI is the lack of datasets suitable for machine learning. This is largely because data acquisition in traditional materials science involves a focus on hypotheses and interests, which is called sampling bias in data science.

Catalysis is often a complicated tangle of multiple elementary reactions, where multicomponent design of solid catalysts provides an opportunity for finer control of a chemical process. The main problem here is that it is extremely difficult to predict the structure of a composite resulting from a combination of multicomponents and its influences on respective elementary reactions. For the multidimensional design of solid catalysts and the multivariate nature of their performance, the data scientific approach, MI, would be very powerful, if a proper dataset was present.

Recently, we have developed a high-throughput experimental setup that can automatically acquire the performance of 20 catalysts at a pre-programmed set of reaction temperatures and gas compositions in a fixed-bed reactor configuration (Figure 1).[1,2] The setup, in conjunction with parallelized catalyst preparation protocols, is usable for collecting catalysts datasets suitable for machine learning in a short time of period. In the presentation, our recent researches on catalytic discoveries based on the high-throughput experimentation and data science methods will be demonstrated.

1) Nguyen, T. N.; Tran, T. P. N.; Takimoto, K.; Thakur, A.; Nishimura, S.; Ohyama, J.; Miyazato, I.; Takahashi, L.; Fujima, J.; Takahashi, K.; Taniike, T. *ACS Catal.* **2020**, *10*, 921– 932.

2) Nguyen, T. N.; Nakanowatari, S.; Tran, T. P. N.; Thakur, A.; Takahashi, L.; Takahashi, K.; Taniike, T. *ACS Catal.* **2021**, *11*, 1797– 1809.T. Taniike, M. Terano, *Macromol. Chem. Phys.* **2009**, *210*, 2118.

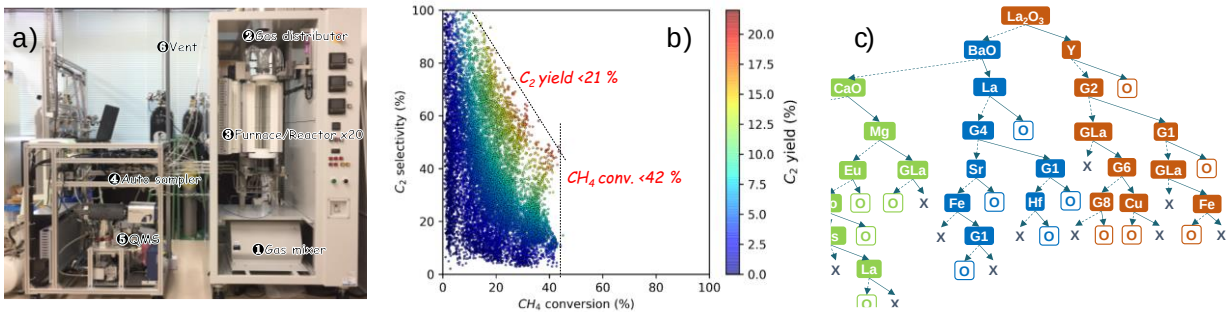

Figure 1. a) Instrument for catalyst screening, b) example of catalyst big data acquired by high-throughput experimentation, and c) example of machine learning where combinatorial design of solid catalyst is learnt.

